THE JOURNAL OF PHYSICAL CHEMISTRY C

Article

pubs.acs.org/JPCC

Reactivity and Selectivity Descriptors for the Activation of C−H Bonds in Hydrocarbons and Oxygenates on Metal Oxides

Prashant Deshlahra[†] and Enrique Iglesia*[,†,‡]

[†]Department of Chemical and Biomolecular Engineering, University of California at Berkeley Berkeley, California 94720, United States

[‡]Chemical Sciences Division, E.O. Lawrence Berkeley National Laboratory, Berkeley, California 94720, United States

Supporting Information

ABSTRACT: C−H bond activation at lattice O atoms on oxides mediates some of the most important chemical transformations of small organic molecules. The relations between molecular and catalyst properties and C−H activation energies are discerned in this study for the diverse C−H bonds prevalent in C_1−C_4 hydrocarbons and oxygenates using lattice O atoms with a broad range of H atom abstraction properties. These activation energies determine, in turn, attainable selectivities and yields of desired oxidation products, which differ from reactants in their C−H bond strength. Brønsted-Evans−Polanyi (BEP) linear scaling relations predict that C−H activation energies depend solely and linearly on the C−H bond dissociation energies (BDE) in molecules and on the H-atom addition energies (HAE) of the lattice oxygen abstractors. These relations omit critical interactions between organic radicals and surface OH groups that form at transition states that mediate the H atom transfer, which depend on both molecular and catalyst properties; they also neglect deviations from linear relations caused by the lateness of transition states. Thus, HAE and BDE values, properties that are specific to a catalyst and a molecule in isolation, represent incomplete descriptors of reactivity and selectivity in oxidation catalysis. These effects are included here through crossing potential formalisms that account for the lateness in transition states in estimates of activation energies from HAE and BDE and by estimates of molecule-dependent but catalyst-independent parameters that account for diradical interactions that differ markedly for allylic and nonallylic C−H bonds. The systematic ensemble-averaging of activation energies for all C−H bonds in a given molecule show how strong abstractors and high temperatures decrease an otherwise ubiquitous preference for activating the weakest C−H bonds in molecules, thus allowing higher yields of products with C−H bonds weaker than in reactants than predicted from linear scaling relations based on molecule and abstractor properties. Such conclusions contradict the prevailing guidance to improve such yields by softer oxidants and lower temperatures, a self-contradictory strategy, given the lower reactivity of such weaker H-abstractors. The diradical-type interactions, not previously considered as essential reactivity descriptors in catalytic oxidations, may expand the narrow yield limits imposed by linear free energy relations by guiding the design of solids with surfaces that preferentially destabilize allylic radicals relative to those formed from saturated reactants at C−H activation transition states.

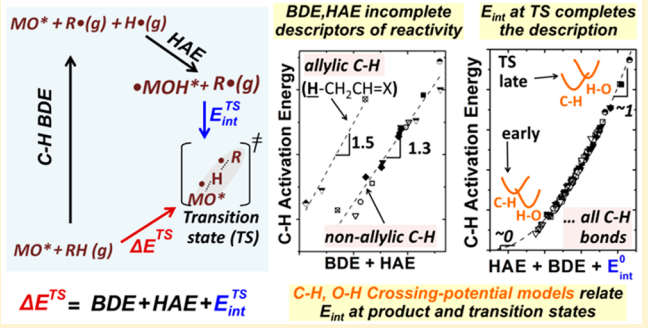

1. INTRODUCTION

Catalytic oxidations in general and oxidative dehydrogenations (ODH) in particular represent essential chemical routes for the conversion of alkanes and alkanols to more valuable molecules.[1−3] These reactions occur at active lattice oxygens on metal oxide surfaces (MO*) via the kinetic coupling of reduction and oxidation elementary steps.[4−6] Kinetic, isotopic, and theoretical studies have shown that such cycles are typically limited by the reduction part of these cycles, which involves H-abstraction from the organic substrate by MO*.[7−9] The resulting reduced centers, present as either OH groups (MOH*) or O-vacancies (M*), then react with O_2(g) in fast and kinetically-irrelevant steps that complete a catalytic turnover.[7−9]

These oxidative routes avoid the energy inefficiencies and significant catalyst deactivation prevalent in their nonoxidative analogs, but attainable yields of desired primary products[1,2] are limited by the sequential oxidation of the desired products to CO and CO_2 (CO_x, Scheme 1); in most cases, such products oxidize more readily than reactants[10,11] because their C−H bond dissociation energies (BDE) are smaller. Brønsted−Evans−Polanyi (BEP) formalisms[12,13] relate activation energies for elementary steps to their reaction energy, causing faster rates for the reactions most favored by thermodynamics.[14] For a given MO* species as the abstractor, a weaker C−H bond will

Received: May 6, 2016
Revised: July 5, 2016
Published: July 20, 2016

DOI: 10.1021/acs.jpcc.6b04604
J. Phys. Chem. C 2016, 120, 16741−16760

Scheme 1. Plausible Pathways for Sequential Oxidative Conversion of Reactant Alkanes (CH_4, C_nH_{2n+2}) and Alkanols ($C_nH_{2n+1}OH$) and Their Primary Alkene (C_nH_{2n}) and Alkanal ($C_nH_{2n}O$) Products on Oxide Catalysts[a]

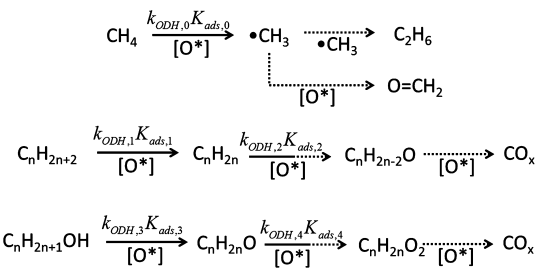

[a]The $k_{ODH}K_{ads}$ values represent rate constants for C−H bond activation reactions, as defined by eq 1. Subscripts 0, 1, 2, 3, and 4 represent C−H activation in CH_4, larger alkanes, alkenes, alkanols, and alkanals, respectively.

be activated via less endothermic routes and exhibit lower barriers than stronger C−H bonds. Such BEP relations have led to empirical expectations (and some experimental evidence) that attainable yields are a single-valued function of BDE differences between the weakest C−H bonds in reactants and products for catalytic oxidations in general.[11]

The supporting quantitative evidence for such reactivity−BDE relations and for their consequences for selectivities and yields are seldom available from theory or experiment in a systematic manner and for broad classes of reactions and catalysts, often placing unreasonable expectations for improved catalytic performance, while also advancing inappropriate reaction conditions and catalyst compositions. For instance, low-temperatures, soft oxidants, and less reactive oxides are often proposed as the most effective routes for higher selectivities and yields, yet such criteria not only are mutually exclusive and actually would lead to low turnover rates and conversions[15] but also favor secondary conversion routes, which involve weaker C−H bonds and thus lower activation barriers.[16] At the higher temperatures and with the strong oxidants that favor high yields of primary products, the prevalence of activation entropies and the early transition states involved weaken the effects of C−H bond energies on reactivity[17] but also lead to the activation of C−H bonds throughout the molecules, instead of only at the weakest C−H bond.[15]

Theoretical treatments are required for a rigorous examination of these effects, including the effects of a broad range of MO* species as H-abstractors, but such assessments require realistic models of solid surfaces and accurate descriptions of complex potential energy surfaces for C−H activation steps.[18−20] They exhibit spin crossings and couplings that require broken-symmetry treatments within density functional theory (DFT) or rigorous multireference methods of inaccessible computational cost,[18,21,22] thus preventing the systematic treatment of the broad range of molecules and abstractors required for useful and accurate composition−function relations.

Keggin polyoxometalate (POM) clusters exhibit well-defined atomic connectivity and represent attractive inorganic models for MO* species as abstractors[23−26] while retaining the compositional flexibility required for abstractors differing in reactivity. Their structure remains intact during alkanol ODH,[9] thus enabling rigorous mechanistic analysis by experiment and theory.[9,27] These studies have shown that H-atom addition energies (HAE) provide reliable descriptors of the stability of the O−H species formed upon C−H activation and, consequently, through BEP relations for steps involving late transition states, also of the effectiveness of specific metal oxides in activating specific C−H bonds in reactants and products.

Here, DFT methods are used to relate activation barriers for C−H bonds in homologous series of alkanes (CH_4, C_2H_6, C_3H_8, C_4H_{10}) and alkanols (CH_3OH, C_2H_5OH, C_3H_7OH) with different chain length and substitution and in the products formed from these reactants (C_2H_4, C_3H_6, C_4H_8, CH_2O, CH_3CHO). These barriers are obtained on POM clusters ($H_3PMo_{12}O_{40}$, $H_4SiMo_{12}O_{40}$, $H_3PW_{12}O_{40}$, $H_4PV_1Mo_{11}O_{40}$, $H_4PV_1W_{11}O_{40}$) at their different O atom locations with different abstractor strengths calculated using DFT,[28] and also using DFT+U[29] methods as a way to heuristically but rigorously expand the range of abstractors. We show that the effects of molecule and catalyst identity on C−H activation barriers depend on the C−H bond dissociation energy of reactants (C−H BDE), on the energy to add an H atom to a given O atom at metal oxide surfaces or to other types of H-abstractors (HAE), and on the interaction energy between the organic radical and the oxide surface, including the OH group formed by H-addition at the transition state (E_{int}^{TS}). These E_{int}^{TS} values depend, in turn, on the magnitude of radical−surface interaction energies (E_{int}°) at the product-state and on the lateness of the relevant transition state, which is estimated using formalisms that represent transition states as the crossing points between harmonic C−H and O−H bond dissociation potentials.[14,30]

These conceptual frameworks and the DFT-derived activation energies demonstrate how radical−surface interactions, not considered in previous analyses, markedly disrupt the monotonic effects of C−H BDE on activation energies inferred from BEP relations. These effects, taken together with the role of H-abstractors in determining the location of transition states along the reaction coordinate and of reaction temperatures in determining enthalpy−entropy trade-offs, provide accurate guidance for the only design parameters that can perturb the pervasive limits in attainable yields imposed by the sequential nature of oxidation reactions that form products with C−H bonds very different in strength from those in reactants.[10,11]

2. COMPUTATIONAL METHODS

The Vienna *ab initio* simulation package (VASP)[31,32] was used to carry out periodic plane-wave density functional theory (DFT) calculations of elementary steps involved in C−H activation within hydrocarbons and oxygenates on polyoxometalate (POM) clusters. Valence electronic states were treated using the Perdew−Wang implementation (PW91)[28] of the exchange−correlation functional based on the generalized gradient approximation and a plane wave basis-set expansion to a cutoff energy of 400 eV. Interactions between valence electrons and atomic cores were described using projector augmented wave (PAW) method.[33] Electronic structures were converged self-consistently to energy differences less than 1×10^{-5} eV between successive iterative steps. Calculations were performed with non-spin-polarized singlet, as well as spin-polarized singlet and triplet, band occupancies to determine the most stable electronic structures, because C−H activation steps exhibit crossings of potential energy surfaces with different spin multiplicities and involve diradical type intermediates and

DOI: 10.1021/acs.jpcc.6b04604
J. Phys. Chem. C 2016, 120, 16741−16760

transition states.[18,20] DFT+U methods were used in some cases to introduce modifications based on Hubbard model[29,34,35] to the Mo d-orbitals. The Hubbard U interactions do not provide better agreement with measured activation energies, as shown previously on similar systems,[27] but they result in more reactive lattice oxygen than those derived from DFT treatments. Therefore, such treatments were used here to broaden the range of catalyst redox properties and specifically of HAE values than those accessible from the range of practical and stable POM compositions.

All calculations were performed on full Keggin POM clusters (diameter ~1.1 nm) placed at the center of $2 \times 2 \times 2$ nm^3 cells to prevent overlap of the electron density among clusters in adjacent cells. Dipole and quadrupole moments, calculated with the center of the unit cell taken as the center of charge, were used to correct for any long-range interactions among neighboring cells. The first Brilliouin zone was sampled using a $1 \times 1 \times 1$ Monkhorst−Pack k-point mesh. The structures of reactants, products, and stable intermediates were optimized until forces on atoms were less than 0.05 eV Å^{-1}.

Minimum energy paths on singlet and triplet potential energy surfaces were calculated using nudged elastic band (NEB) methods[36] to determine likely transition state structures. These likely structures were then used to isolate transition states using the Henkelman's dimer method.[37] The electronic and geometric steps in NEB calculations were converged to energy changes less than 1×10^{-5} eV and to forces on all atoms less than 0.1 eV Å^{-1}, respectively. The respective convergence criteria for dimer calculations were 1×10^{-7} eV for energies and 0.05 eV Å^{-1} for forces.

Vibrational frequencies were calculated by diagonalizing second-derivative matrices computed from two-sided finite differences of energy gradients obtained by perturbing each atom in organic molecules and in Mo_2O_3 fragments nearest to the O atom used in C−H bond activation in all three Cartesian directions by ±0.01 Å. Enthalpies, entropies, and Gibbs free energies were determined from electronic energies, zero-point vibrational energies, and contributions from translational, rotational, and vibrational degrees of freedom determined using statistical mechanics formalisms.[27,38] Low-frequency modes (less than ~100 cm^{-1}) of weakly bound C−H activation transition states lead to significant inaccuracies in the vibrational contributions[27] and, therefore, were excluded from thermodynamic partition functions.[27] Their contributions were instead determined by assuming that they retain a fraction (0.7) of the translational and rotational contributions to entropies and enthalpies per mode estimated by statistical mechanics for gaseous reactants. These choices were motivated by experimental data that show that molecules adsorbed on well-defined oxide surfaces retain approximately 0.7 of their entropy as gaseous species.[39] Detailed listing of vibrational frequencies and values of thermodynamic contributions from each mode are shown for CH_3OH in previous studies.[27] Such details for CH_4, C_3H_8, and C_3H_6 activation and the effect of varying the 0.7 factor (between 0 and 1) on ratios of C−H activation rate constants are shown in the Supporting Information.

The results reported in the Supporting Information (section S2, Table S1, Figures S2 and nS3) contrast the trends in C−H BDE, HAE, and C−H activation energies shown here (VASP, PW91 functionals, plane-wave basis sets) with those derived from hybrid-DFT methods and localized atomic basis sets within the Gaussian program[40] (details in Supporting Information). These comparisons show that (i) all Gaussian-derived C−H BDE values are consistently higher than corresponding VASP values by 12 ± 2 kJ mol^{-1}, (ii) POM HAE values derived from Gaussian are more negative than VASP values (by −11 to −44 kJ mol^{-1}), and (iii) activation energies as a function of HAE + BDE values show the same trends for VASP and Gaussian derived values with similar offsets between allylic and nonallylic C−H bonds.

3. RESULTS AND DISCUSSION

3.1. Mechanistic Details and Thermochemical Cycle Descriptions of Dehydrogenation (ODH) Reactions. The measured effects of reactant pressures (P_{RH}) on turnover rates for ODH reactions of hydrocarbons and oxygenates are accurately described by an equation that contains the equilibrium constant for reactant adsorption (K_{ads}) and the rate constant for irreversible H-abstraction from adsorbed reactants by a lattice oxygen (k_{ODH}):[7−9,15]

$$\frac{r_{ODH}}{[L]} = \frac{k_{ODH}K_{ads}P_{RH}}{1 + K_{ads}P_{RH}} \quad (1)$$

where $[L]$ is the total number of reactive sites. The weak nature of molecular adsorption of alkanes causes rates to remain proportional to their pressure at most practical conditions ($K_{ads}P_{RH} \ll 1$).[7,8] Oxygenates bind somewhat more strongly via H-bonding, thus causing rates to approach constant values as $K_{ads}P_{RH}$ increases.[9] For both reactants, first-order rate constants ($k_{ODH}K_{ads}$) reflect the free energy of a kinetically-relevant transition state (G^{TS}) relative to an uncovered catalyst surface with stoichiometric amounts of lattice O atoms (G^{MO*}) and a gaseous reactant molecule ($G^{RH(g)}$),

$$k_{ODH}K_{ads} \approx \exp\left(\frac{-G^{TS} - G^{MO*} - G^{RH(g)}}{RT}\right) = \exp\left(\frac{-\Delta G^{TS}}{RT}\right) \quad (2)$$

Deuterated reactants exhibit lower rates than those containing protium,[7−9] which, taken together with theoretical treatments of energies and free energies for elementary steps,[27] show that H-abstraction from molecularly adsorbed reactants is the sole kinetically-relevant step for all these reactants.

C−H activation steps may occur via several plausible routes in both the reactants and the intended (and typically desired) primary products (Scheme 1). The maximum attainable selectivities to primary products (at a given conversion) in such sequential reactions reflect the ratios of first-order rate constants for primary and secondary reactions (χ_1, χ_2 in reactions of hydrocarbons and oxygenates, respectively), given by the corresponding activation free energies:[15]

$$\chi_1 = \frac{k_{ODH,1}K_{ads,1}}{k_{ODH,2}K_{ads,2}} = e^{-(\Delta G^{TS_1} - \Delta G^{TS_2})/(RT)} \quad (3)$$

$$\chi_2 = \frac{k_{ODH,3}K_{ads,3}}{k_{ODH,4}K_{ads,4}} = e^{-(\Delta G^{TS_3} - \Delta G^{TS_4})/(RT)} \quad (4)$$

A thermochemical cycle, such as the one shown in Scheme 2, can be used to describe how activation energies of individual C−H activation reactions in sequential ODH pathways depend on properties of reactants and oxide catalysts. Such formalisms, previously used to develop reactivity descriptors in acid-catalyzed reactions on solids,[41−43] rigorously dissect the

DOI: 10.1021/acs.jpcc.6b04604
J. Phys. Chem. C 2016, 120, 16741−16760

Scheme 2. Thermochemical Cycle Description of the C−H Activation Transition-State Energy Relative to a Gaseous Organic Reactant and a Surface Metal Oxide Site (MO*) as a Sum of (i) the Energy Required to Separate H Atom from the C Atom in the Reactant to Form a Radical Species (C−H BDE), (ii) the Energy of Adding the H Atom to the O Atom of MO* (HAE), and (iii) Interaction Energy between the Radical (R•) and Hydroxylated Metal Oxide (•MOH*) at the Transition State (E_{int}^{TS})

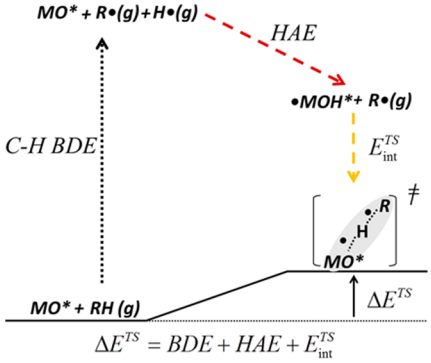

individual interactions and energies that contribute to transition state energies and activation barriers by exploiting the state function character of the relevant thermodynamic properties.[44] For the activation of C−H bonds in gaseous molecules by lattice O atoms on oxide surfaces (eqs 1 and 2), these hypothetical steps can be conveniently assembled as (i) the dissociation of the C−H bond in the gaseous molecule to form the H and organic free radicals at an energy cost that is a molecular property insensitive to the identity of the catalyst (C−H BDE), (ii) the addition of the H atom formed to an O atom in the oxide to form a surface OH species to recover an energy that depends on the catalyst properties but not on the identity of the reactant molecule (HAE), and (iii) the placement of the organic radical in step i near the OH species in step ii to form the transition state structure, thus recovering an interaction energy that depends on the properties of both the reactant and the catalyst (E_{int}^{TS}).

These steps are shown in the thermochemical cycle in Scheme 2, which allows the activation energy (ΔE^{TS}) to be expressed as the sum of the energies for the hypothetical steps i−iii:

$$\Delta E^{TS} = BDE + HAE + E_{int}^{TS} \quad (5)$$

This relation indicates that activation energies will be lower for reactants with lower C−H BDE and catalysts with more negative HAE, as also predicted by Brønsted−Evans−Polanyi (BEP) relations that link activation energies with the energy for a particular reaction step. The trends in activation energy also depend, however, on radical−surface interactions at the transition states and on their concomitant sensitivity to the properties of the reactant and of the catalyst sites involved in the specific step. We explore such dependencies here for C−H bonds in alkanes, alkenes, alkanols, and alkanals, which are involved in the primary and secondary reactions depicted in Scheme 1. We do so specifically for their activation on POM clusters, which are used here without loss of generality because such clusters provide a broad range of the surface properties that encompass those of most practical oxidation catalysts, which, as in the case of POM, consist of metal cations surrounded by oxygen anions in 6-fold octahedral coordination.[45] In doing so, we show how simplistic scaling relations represent incomplete, and often distracting, descriptions of reactivity, even for the oxidation of small reactant and product molecules.

We proceed by first examining how DFT-derived C−H BDE and HAE values depend on the identity of the reactants and the POM clusters, respectively, and exploring C−H activation potential energy surfaces to isolate accurate transition state structures and energies, which are then used for thermochemical analyses.

3.2. C−H Bond Dissociation Energies in Reactants and Hydrogen Addition Energies (HAE) at Lattice Oxygens.

DFT-derived standard enthalpies (ΔH°_{C-H}) for the dissociation of the weakest C−H bonds in small alkanes and alkanols and in the alkenes and alkanals formed by their respective dehydrogenations are shown in Table 1. Dissociation enthalpies

Table 1. DFT-Derived Electronic Energies (without Zero-Point Energy Correction) and Enthalpies (at 298.15 K and 101.325 kPa) for Dissociation of C−H Bonds in Hydrocarbons and Oxygenates

molecule	C−H bond	ΔE_{C-H}, DFT (kJ mol^{-1})	ΔH_{C-H}, DFT (kJ mol^{-1})
	Alkanes		
CH_4	CH_4	465	433
C_2H_6	CH_3CH_3	442	410
C_3H_8	$CH_3CH_2CH_3$	427	394
	$CH_3CH_2CH_3$	443	412
i-C_4H_{10}	$(CH_3)_2CHCH_3$	411	380
	$(CH_3)_2CHCH_3$	444	413
n-C_4H_{10}	$CH_3CH_2CH_2CH_3$	426	394
	$CH_3CH_2CH_2CH_3$	442	410
	Alkanols		
CH_3OH	CH_3OH	417	387
C_2H_5OH	CH_3CH_2OH	406	377
	CH_3CH_2OH	448	416
C_3H_7OH	$(CH_3)_2CHOH$	402	372
	$(CH_3)_2CHOH$	451	419
	Alkenes		
C_2H_4	$CH_2=CH_2$	480	448
C_3H_6	$CH_2=CHCH_3$	480	450
	$CH_2=CHCH_3$	458	425
	$CH_2=CHCH_3$	371	342
1-C_4H_8	$CH_2=CHCH_2CH_3$	356	326
	Alkanals		
CH_2O	$CH_2=O$	385	357
CH_3CHO	$CH_3CH=O$	385	360
	$CH_3CH=O$	411	383

decrease among alkanes from 433 kJ mol^{-1} for a H atom bound to an isolated methyl group in CH_4 ($\Delta H^{\circ}_{CH_4}$) to 380 kJ mol^{-1} for the C−H bond at the tertiary C atom in isobutane ($\Delta H^{\circ}_{(CH_3)_3CH}$), consistent with a greater stability of organic radicals formed upon dissociation at more substituted C atoms. Alkanols show analogous effects of C atom substitution (a decrease from $\Delta H^{\circ}_{CH_3OH}$ = 387 kJ mol^{-1} for a H atom at the methyl group in CH_3OH group to $\Delta H^{\circ}_{(CH_3)_2CHOH}$ = 372 kJ mol^{-1} at the secondary C atom in isopropanol). The dissociation enthalpies in alkanols are smaller and lie within a narrower range than those for alkanes, indicating that O-substituents stabilize the radicals formed upon C−H cleavage

DOI: 10.1021/acs.jpcc.6b04604
J. Phys. Chem. C 2016, 120, 16741−16760

more effectively that C-substituents. Alkene products have stronger C−H bonds at the C atoms connected by the π-bond formed ($\Delta H^{\circ}_{CH_2=C\underline{H}CH_3}$ = 425 kJ mol^{-1}, $\Delta H^{\circ}_{CH_3C\underline{H}_2CH_3}$ = 394 kJ mol^{-1}) but much weaker C−H bonds at allylic C atoms ($\Delta H^{\circ}_{CH_2=CHC\underline{H}_3}$ = 342 kJ mol^{-1}) than the alkanes from which they form. In contrast, alkanals show weaker C−H bonds at the carbonyl group than the alkanol reactants ($\Delta H^{\circ}_{C\underline{H}_3=O}$ = 357 kJ mol^{-1}, $\Delta H^{\circ}_{C\underline{H}_3OH}$ = 387 kJ mol^{-1}). C−H bonds allylic to carbonyl groups in alkanals are weaker than the bonds at the equivalent position in the reactant alkanols ($\Delta H^{\circ}_{C\underline{H}_3CH=O}$ = 383 kJ mol^{-1}, $\Delta H^{\circ}_{C\underline{H}_3CH_2OH}$ = 419 kJ mol^{-1}) but much stronger than the bonds at carbonyl and hydroxyl groups in alkanals and alkanols, respectively ($\Delta H^{\circ}_{CH_3C\underline{H}=O}$ = 360 kJ mol^{-1}, $\Delta H^{\circ}_{CH_3C\underline{H}_2OH}$ = 377 kJ mol^{-1}). These trends are consistent with experimental bond-dissociation enthalpies,[46] as shown by the comparison between DFT-derived and experimental BDE values in Figure 1. DFT-derived values are 5−20 kJ mol^{-1} smaller than those measured but show similar effects of substitution and similar energy differences among C−H bonds in different molecules.

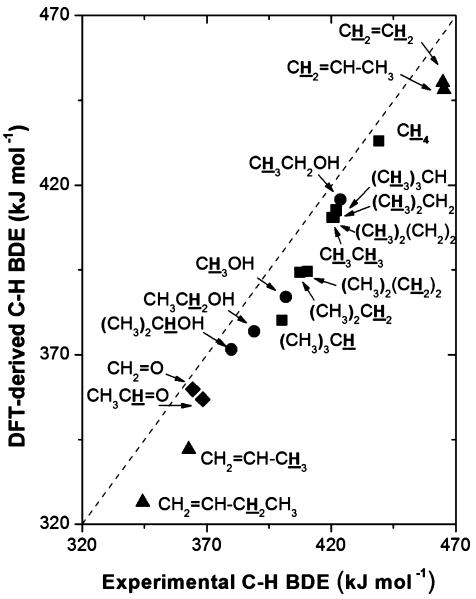

Figure 1. DFT-derived C−H bond dissociation energies (ΔH° values, Table 1) in alkanes (■), alkanols (●), alkenes (▲), and alkanals (◆) as a function of corresponding experimental values.[46] Dashed line represents the parity line. H designates the specific C−H bond being cleaved.

The calculated C−H bond dissociation electronic energies (ΔE_{C-H}, Table 1) are slightly larger (by 30−33 kJ mol^{-1}) than the corresponding enthalpies (ΔH°_{C-H}), indicating that corrections for zero-point vibrational energies[38] and thermal contributions to enthalpy[38] are similar for all C−H bonds and thus rendering relative energies and enthalpies similar to each other. Henceforth, the bond dissociation energy (BDE) for a given C−H bond refers to its ΔE_{C-H} values, and we probe the effects of ΔE_{C-H} values on the ΔE^{TS} barriers required to form the C−H activation transition states. The ΔE^{TS} values are then used to derive free energies and rate constants using statistical mechanics treatments by using appropriate corrections for low-frequency vibrational modes in the weakly bound transition states.[39]

DFT-derived H-atom addition energies (HAE) on POM clusters vary with the location of the O atoms in a given cluster (Figure 2, Table 2; −313 to −253 kJ mol^{-1} at locations 1

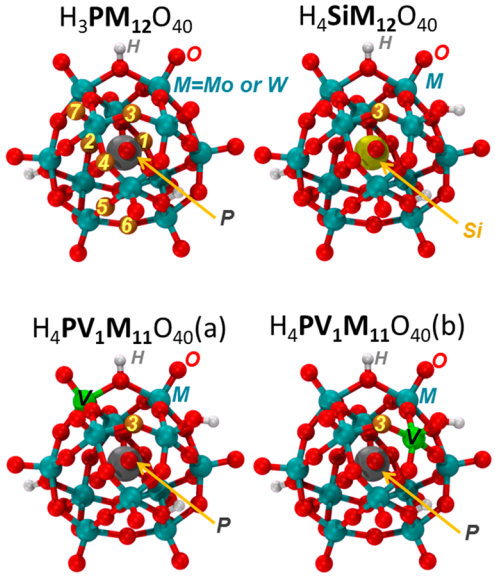

Figure 2. POM cluster structures and the locations of the O atoms used to activate C−H bonds for each cluster composition (adapted from ref 27, Figure 6c).

Table 2. H-Atom Addition Energy (HAE, without Zero-Point Energy Corrections) Derived from DFT and DFT+U Methods at Different O Atoms on POM Clusters Shown in Figure 2

POM cluster	O atom location[b]	O atom type	Method[a]	HAE (kJ mol^{-1})
$H_3PMo_{12}O_{40}$	1	Mo−O−Mo	DFT	−313
$H_3PMo_{12}O_{40}$	2	Mo−O−Mo	DFT	−307
$H_3PMo_{12}O_{40}$	3	Mo−O−Mo	DFT	−295
$H_3PMo_{12}O_{40}$	4	Mo−O−Mo	DFT	−282
$H_3PMo_{12}O_{40}$	5	Mo−O−Mo	DFT	−277
$H_3PMo_{12}O_{40}$	6	Mo−O−Mo	DFT	−266
$H_3PMo_{12}O_{40}$	7	Mo=O	DFT	−253
$H_3PMo_{12}O_{40}$	3	Mo−O−Mo	DFT+U (U = 6.0)	−320
$H_3PMo_{12}O_{40}$	3	Mo−O−Mo	DFT+U (U = 7.0)	−336
$H_3PMo_{12}O_{40}$	3	Mo−O−Mo	DFT+U (U = 7.5)	−344
$H_3PMo_{12}O_{40}$	3	Mo−O−Mo	DFT+U (U = 8.0)	−356
$H_3PW_{12}O_{40}$	3	W−O−W	DFT	−227
$H_4SiMo_{12}O_{40}$	3	Mo−O−Mo	DFT	−286
$H_4PV_1Mo_{11}O_{40}$ (a)	3	Mo−O−Mo	DFT	−280
$H_4PV_1Mo_{11}O_{40}$ (b)	3	Mo−O−V	DFT	−297
$H_4PV_1W_{11}O_{40}$ (a)	3	W−O−W	DFT	−196
$H_4PV_1W_{11}O_{40}$ (b)	3	W−O−V	DFT	−253

[a]U values were applied to Mo d-orbitals. [b]Atom locations defined in Figure 2.

DOI: 10.1021/acs.jpcc.6b04604
J. Phys. Chem. C 2016, 120, 16741−16760

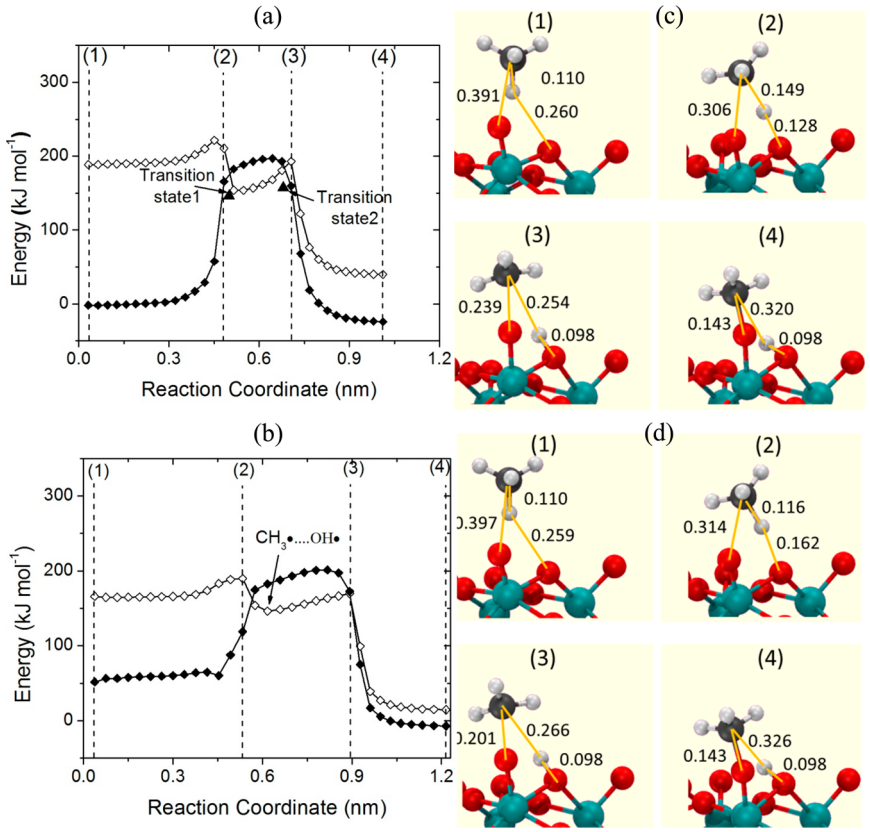

Figure 3. Singlet (◆) and triplet (◇) state energies of molecular images along the C−H activation reaction coordinate derived from nudged-elastic band (NEB) calculations performed on (a) a singlet potential energy surface and (b) triplet potential energy surface (PES) for C−H activation in CH_4 on $H_3PMo_{12}O_{40}$ cluster. The triangles (▲) near PES crossings represent energies of transition states obtained from dimer calculations with spin-polarized singlet states. Geometries of images 1 through 4 in panels a and b are shown in panels c and d, respectively.

through 7 in $H_3PMo_{12}O_{40}$) and with the POM composition for a given O atom location (Figure 2, Table 2; −297 to −196 kJ mol^{-1} at location 3 on Mo and W addenda atom based POM clusters with and without substitution of one addenda atom by a V atom). Location 3 was chosen for transition state calculations for clusters with varying composition changes because it remains adjacent to a V atom in V-substituted POM clusters. The choice is otherwise arbitrary and in no way affects the comparisons as long as it is used consistently. The HAE values at a given location in $H_3PMo_{12}O_{40}$ clusters are more negative when DFT+U (instead of DFT) is used, because such treatments introduce corrections to interactions among Mo d-orbitals in the POM cluster based on the Hubbard model and an ad hoc value of U parameter;[29] these corrections lead to more negative HAE values and lower C−H activation energies for a given value of U used to calculate both HAE and C−H activation transition state energies. U values of 6 and 8 eV led to much more negative HAE values (−320 and −356 kJ mol^{-1} for site 3, $H_3PMo_{12}O_{40}$; Table 2) than those from DFT treatments (−295 kJ mol^{-1}). Thus, different O atom locations, different POM compositions, and different U values in DFT+U methods lead to a broad range of H-abstractors with very different potency (HAE values from −356 to −196 kJ mol^{-1}).

Next, we probe activation pathways for a set of diverse hydrocarbons and oxygenates on the O atom exposed on such surfaces to identify intermediates and transition states relevant to the measured rate constants described in Scheme 1 and eqs 1−4.

3.3. C−H Activation Pathways in Hydrocarbons and Oxygenates.

The reactants and products in C−H activation processes on oxides can have different spin multiplicities in their most stable electronic ground states.[18,20] These differences lead to a crossing between potential energy surfaces for singlet (no unpaired electrons) and triplet (two unpaired electrons) states along the reaction coordinate. The molecular structures near such crossings benefit from spin-coupling effects, which lead, in turn, to new broken-symmetry states with energies lower than for either singlet or triplet states.[18,20] We explore such effects here by examining the minimum energy path (MEP) for each multiplicity, derived here from nudged elastic band (NEB) calculations[36] in the manner described in the Computational Methods section.

3.3.1. C−H Activation in CH_4 on Lattice O Atoms. Figure 3a shows the MEP derived from singlet NEB calculations for C−H cleavage in CH_4 at a bridging O atom in $H_3PMo_{12}O_{40}$ clusters and for the subsequent adsorption of the CH_3 radical formed at an adjacent terminal O atom; it also shows triplet energies derived from single-point (unrelaxed) calculations at each point along this MEP. Figure 3b shows the result of an analogous calculation where the MEP was derived instead from a triplet NEB calculation and the singlet energies were derived from single-point calculations. Thus, both figures show the same reaction step, but the singlet energies are minimized in Figure 3a, while the triplet energies are minimized in Figure 3b.

The energies for the singlet and triplet states cross twice along the reaction coordinate for C−H activation in CH_4 molecules. The singlet state energy of the system with an intact

DOI: 10.1021/acs.jpcc.6b04604
J. Phys. Chem. C 2016, 120, 16741−16760

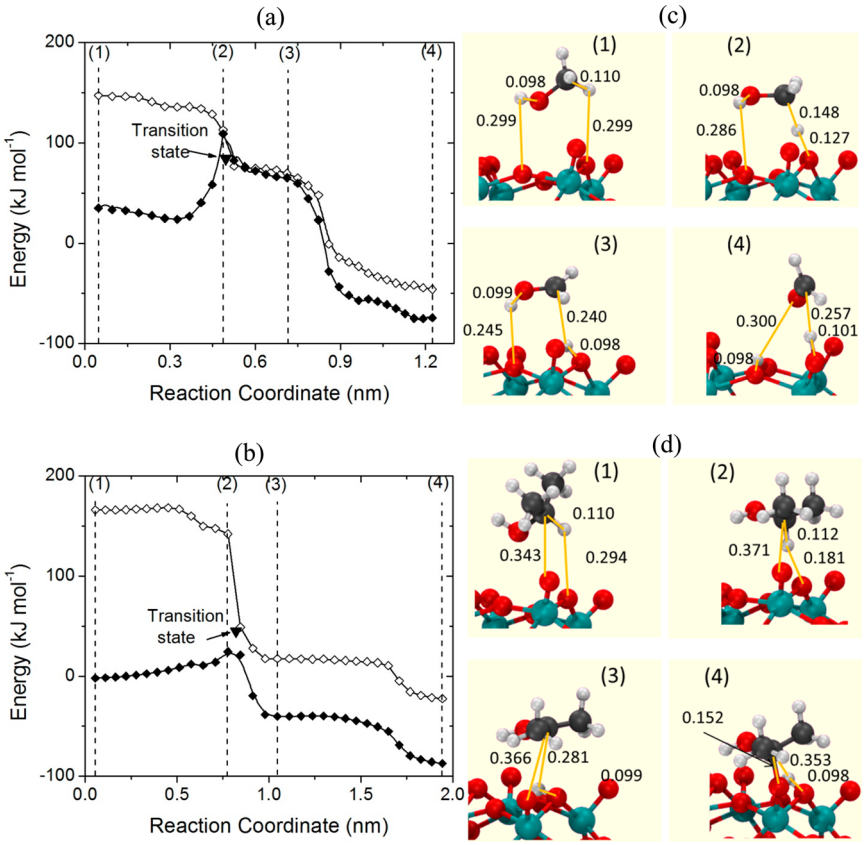

Figure 4. Singlet (◆) and triplet (◇) state energies of molecular images along the C−H activation reaction coordinate derived from nudged-elastic band (NEB) calculations performed on (a) a triplet potential energy surface for C−H activation in CH_3OH on $H_3PMo_{12}O_{40}$ cluster and (b) singlet potential energy surface for C−H activation in C_3H_7OH. The triangles (▼) near PES crossings represent energies of transition states obtained from dimer calculations with spin-polarized singlet states. Geometries of images 1 through 4 in panels a and b are shown in panels c and d, respectively.

CH_4 and an intact POM cluster is 166 kJ mol^{-1} lower than its triplet state. This energy increases sharply and then reaches a nearly constant value as the H atom is separated from the C atom in CH_4 and the O−H bond starts to form at the lattice O atom; the singlet energy then decreases as the CH_3 radical approaches an adjacent lattice O atom to form the O−CH_3 product of the C−H activation elementary step. In contrast, the triplet state energy increases and then decreases only slightly along the reaction coordinate and exhibits a local minimum when the CH_3 radical formation and the O−H bond formation are complete. This triplet energy then increases slightly before decreasing to the value for the bound O−CH_3 species. While CH_4 reactants and bound O−CH_3/H−O products are more stable in their singlet states, the triplet state is the lowest energy form of the CH_3 radical near a hydroxylated POM cluster ($^{\bullet}CH_3\cdots{}^{\bullet}MOH^*$).

These treatments show that the highest energy along the reaction coordinate corresponds to the singlet−triplet crossing point. A transition state could not be located at such crossing points when dimer calculations[37] were performed using spin-restricted singlet or spin-polarized triplet occupancies. The dimer calculations converged, however, to a broken-symmetry open-shell state in a spin-polarized singlet calculation when the structure present immediately after the first crossing point in Figure 3b was used as the starting structure for the transition state search. The energy of this converged transition state (shown as triangles in Figure 3) is smaller than that at the crossing point of the singlet and triplet PES, consistent with a stabilizing effect of the coupling between the two spins in the open-shell electronic configuration[20] and with the diradical-type species prevalent in C−H activation transition states on oxides.[18,19] The energies of converged transition state geometries determined from spin-restricted singlet and spin-polarized triplet single-point calculations were higher than the converged spin-polarized singlet energy (values shown in the Supporting Information). These results further confirm that the calculated transition is in a broken symmetry state that lies at a lower energy than either singlet or triplet states.

Thus, a closed-shell singlet state CH_4 reactant converts to a triplet state CH_3 radical−surface hydroxide pair ($^{\bullet}CH_3\cdots{}^{\bullet}MOH^*$) via an open-shell singlet C−H activation transition state. The CH_3 radical species formed in this elementary step can plausibly form O−CH_3 species via a second broken-symmetry transition state (transition state 2 in Figure 3a,b) or directly couple with another CH_3 species to form C_2H_6 (Scheme 1). The calculated O−CH_3 formation transition state has a higher energy (157 kJ mol^{-1}) than the C−H activation transition state (146 kJ mol^{-1}), which, taken together with the entropic penalty of retaining the CH_3 bound to the surface, makes the gas-phase coupling of CH_3 radicals favored.[47] We focus on the activation energy for the primary C−H activation in our further analyses because it is the kinetically-relevant process in catalytic oxidation practice.

As in the case of CH_4, all other reactant molecules have lower energies in their singlet than in their triplet states. The difference between triplet and singlet energies in radical species formed after C−H activation, however, becomes less negative for the activation of weaker C−H bonds, such as those (shown

DOI: 10.1021/acs.jpcc.6b04604
J. Phys. Chem. C 2016, 120, 16741−16760

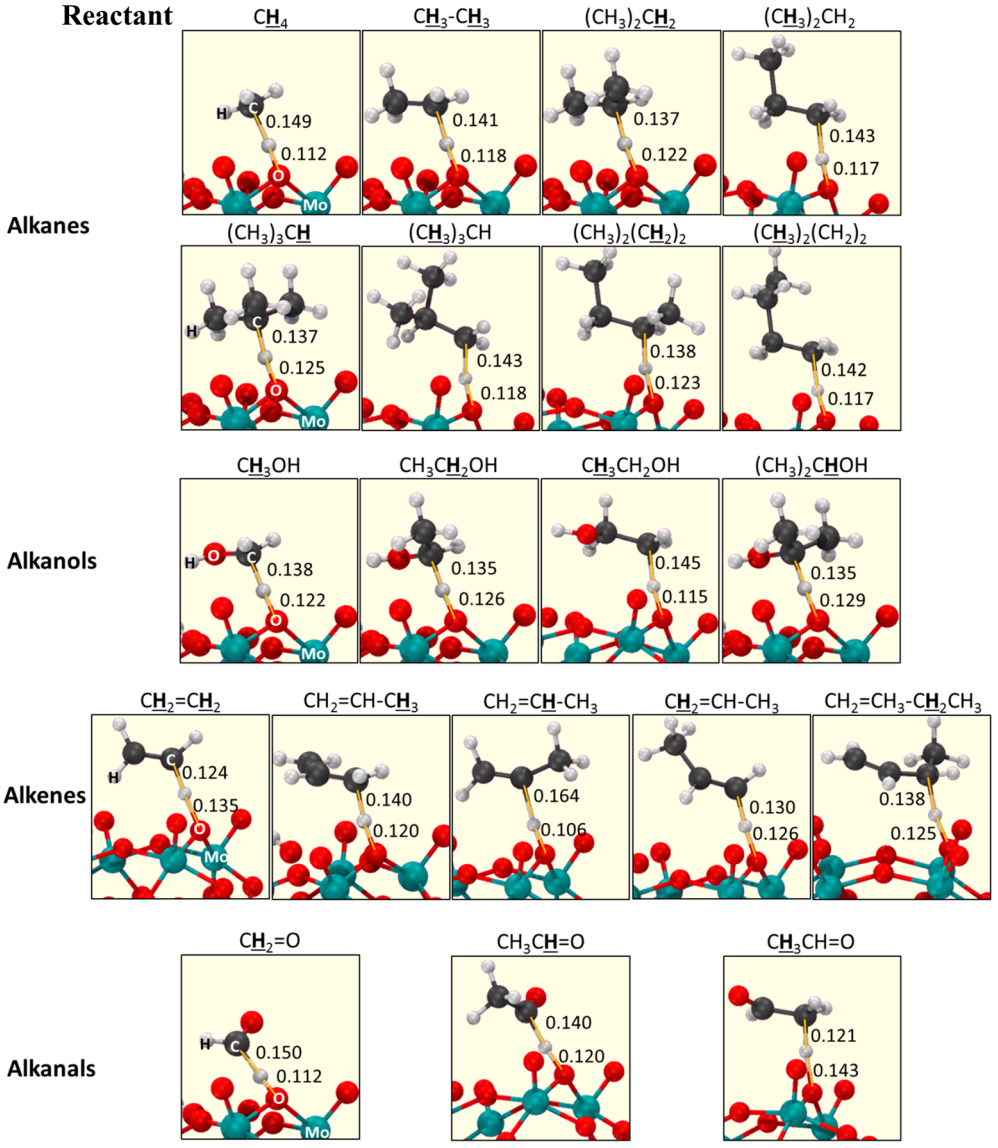

Figure 5. Structures and C−H and H−O bond distances (in nm) at the transition states that mediate C−H bond activation in hydrocarbon and oxygenate reactants at location 3 in $H_3PMo_{12}O_{40}$ clusters (Figure 2).

with bold H atoms) in CH_3CH_3, CH_3OH, and $(CH_3)_2CHOH$ (BDE values in Table 1). When C−H bonds become sufficiently weak, the spin-crossing after C−H activation is completely avoided and all transition states exist as closed-shell singlets. All molecules with C−H bonds weaker than those in CH_4 have lower barriers for the adsorption of their organic radicals on surface O atoms or for the activation of a second C−H bond in such radicals (or their bound analogs) than for the initial C−H activation in reactants, making the initial C−H activation the sole kinetically-relevant step. Such effects of C−H BDE on potential energy surfaces for C−H activation are illustrated next using the minimum energy reaction paths for the activation of CH_3OH and $(CH_3)_2CHOH$ reactants.

3.3.2. C−H Activation in CH_3OH and 2-C_3H_7OH on Lattice O Atoms. CH_3OH ODH reactions on oxides with octahedral metal−oxygen coordination, which are found in most redox oxides reactive for redox reactions,[45] involve direct C−H activation in molecularly adsorbed CH_3OH, instead of an intervening dissociation to form methoxy species before C−H activation.[9,27] The MEP results derived from a triplet state NEB calculation for such direct C−H activation steps in CH_3OH at a bridging O atom in $H_3PMo_{12}O_{40}$ and for the activation of the O−H bond in the CH_2OH radical formed at an adjacent bridging O atom are shown together with singlet state energies of the converged NEB structures in Figure 4a. Singlet and triplet states have similar energies near the highest energy point along the MEP, leading to spin coupling and to broken-symmetry transition states (shown by a triangle in Figure 4a).

Isopropanol ODH reactions also proceed via direct C−H activation in molecular reactants ($(CH_3)_2CHOH$) because steric effects prevent isopropoxy formation at octahedral centers in metal oxides, as for the case of methoxy formation on POM clusters.[9,27] The MEP results derived from a singlet NEB calculation for the activation of the C−H bond in $(CH_3)_2CHOH$ at bridging O atoms in $H_3PMo_{12}O_{40}$ and for the adsorption of $(CH_3)_2COH$ radicals formed at an adjacent terminal O atom are shown together with the triplet state energies of converged NEB structures in Figure 4b. The singlet energy is lower than the triplet energy throughout the reaction coordinate; the transition state derived from the highest point

DOI: 10.1021/acs.jpcc.6b04604
J. Phys. Chem. C 2016, 120, 16741−16760

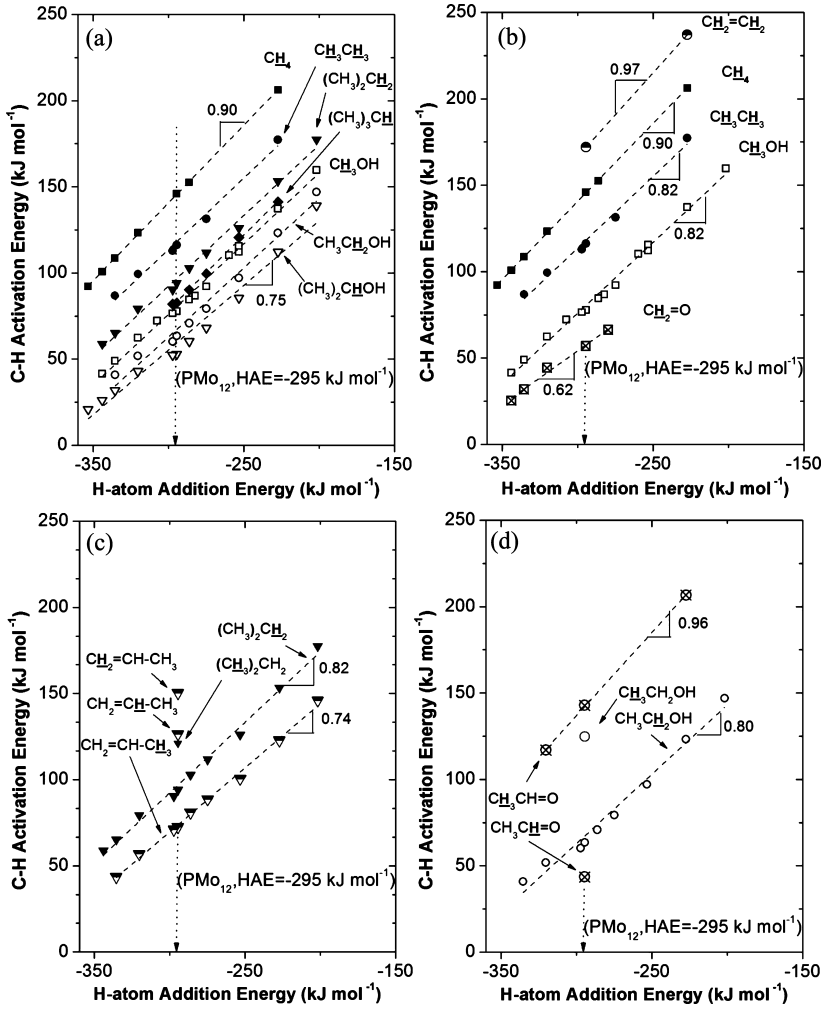

Figure 6. DFT-derived energies of activation of (a) weakest C−H bonds in alkanes and alkanols and all C−H bonds in (b) CH_4, C_2H_6, CH_3OH, and their primary products (C_2H_4, CH_2O), (c) C_3H_8 and C_3H_6, and (d) CH_3CH_2OH and CH_3CHO, as a function of H-atom addition energy (HAE) on POM clusters. Alkanes, alkanols, alkenes, and alkanals are represented by closed, open, half-filled, and crossed symbols, respectively. Dashed lines represent best-fits to activation energies for each molecule. Dotted vertical arrow shows the HAE value at location 3 in $H_3PMo_{12}O_{40}$ clusters (Figure 2). Triangles adjoining the trend lines represent their slopes.

along the MEP converged as a closed-shell singlet TS, even when isolated using spin-unrestricted calculations (shown by a triangle in Figure 4b).

These spin coupling effects, shown here in detail for $C\underline{H}_4$, $C\underline{H}_3OH$, and $(CH_3)_2C\underline{H}OH$ activations but also found for most C−H bonds activated on POM clusters and other oxides,[18,19] require calculations of the singlet and the triplet MEP for all C−H bonds in all reactants. C−H activation transition states must be treated using spin-polarized dimer calculations with singlet multiplicities when broken-symmetry states exist. When C−H bonds in reactants are much stronger than in $C\underline{H}_4$, as in the case of $C\underline{H}_2{=}C\underline{H}_2$ (Table 1; $\Delta E_{C\underline{H}_4}$ = 464 kJ mol−1, $\Delta E_{C\underline{H}_2=C\underline{H}_2}$ = 480 kJ mol^{-1}), the singlet−triplet crossing occurs before the triplet MEP reaches a maximum, leading to transition states with triplet multiplicity, which are treated here using spin-polarized dimer calculations with triplet multiplicities. These effects were rigorously considered by examining overlaps between singlet and triplet MEP and by performing broken-symmetry calculations to obtain accurate C−H activation energies for all C−H bonds on all POM clusters.

The geometries of converged transition states for all C−H bonds in C_1−C_4 alkanes (CH_4, C_2H_6, C_3H_8, *i*-C_4H_{10}, *n*-C_4H_{10}), in C_1−C_3 alkanols (CH_3OH, C_2H_5OH, 2-C_3H_7OH), and in the primary products formed from each of these reactants (C_2H_4, C_3H_6, 1-C_4H_8, CH_2O, CH_3CHO) are shown in Figure 5 for reactions on $H_3PMo_{12}O_{40}$ clusters. Each transition state shows a larger C−H distance (0.124−0.164 nm) than in the C−H bond of its respective gaseous reactants (0.110 nm), and an O−H distance (0.143−0.106 nm) that approaches that in the product state (0.098 nm). Typically, C−H distances are larger and O−H distances are smaller for transition states involved in activating stronger C−H bonds than for those that mediate the activation of weaker C−H bonds. These longer C−H bond and shorter O−H bond distances represent transition states that occur later along the reaction coordinate for the activation of stronger C−H bonds.

Next, we assess how activation energies for the diverse C−H bonds in the molecules shown in Figure 5 and Table 1 vary with changes in their BDE and in the HAE values of the O atoms used as H-abstractors. We interpret these changes within the framework described by the thermochemical cycle in Scheme 2 to propose reactivity descriptors for C−H activation

DOI: 10.1021/acs.jpcc.6b04604
J. Phys. Chem. C 2016, 120, 16741−16760

based on C−H BDE, abstractor HAE, and radical−surface interactions. This systematic treatment shows how their relative contributions to reactivity depend sensitively on the lateness of each specific transition state, which varies, in turn, with the energy of the specific reaction step as prescribed by crossing potentials formalisms.

3.4. Effects of Hydrogen Addition Energy (HAE) at Lattice O Atoms and of C−H Bond Dissociation Energies (BDEs) on C−H Activation Energies. Activation energies for the weakest C−H bond in each reactant alkane ($C\underline{H}_4$, $C\underline{H}_3C\underline{H}_3$, $(CH_3)_2C\underline{H}_2$, $(CH_3)_3C\underline{H}$; 465−411 kJ mol^{-1} C−H BDE, Table 1) and alkanol ($C\underline{H}_3OH$, $CH_3C\underline{H}_2OH$, $(CH_3)_2C\underline{H}OH$; 417−402 kJ mol^{-1} C−H BDE) are shown in Figure 6a as a function of the HAE value of the lattice O atom used to abstract the H atoms from each reactant. More negative HAE values represent stronger O−H bonds in products, which results in lower activation energies for a given C−H bond, as expected from Brønsted−Evans−Polanyi (BEP) relations that predict lower activation energies for less endothermic reactions.[12,13] At a given HAE, weaker C−H bonds in each homologous series (alkanes, alkanols) exhibit lower activation energies because of the less endothermic nature of their activation steps.

Figure 6b shows activation energies as a function of the HAE values of lattice O atoms for the reactions of C−H bonds in $C\underline{H}_4$, $C\underline{H}_3C\underline{H}_3$, and $C\underline{H}_3OH$ reactants (465, 442, and 417 kJ mol^{-1} C−H BDE, respectively) and in the alkenes ($C\underline{H}_2$=$C\underline{H}_2$, 480 kJ mol^{-1} C−H BDE) and alkanals ($C\underline{H}_2$=O, 385 kJ mol^{-1} C−H BDE) that form as their primary products. $C\underline{H}_2$=$C\underline{H}_2$ species have a higher activation energy than $C\underline{H}_3C\underline{H}_3$ molecules at an O atom with a given HAE (172 and 116 kJ mol^{-1} ΔE^{TS}, respectively, at location 3 in $H_3PMo_{12}O_{40}$ cluster; Figure 2), consistent with the stronger C−H bonds at C atoms linked by a π-bond. In contrast, the activation energy for $C\underline{H}_2$=O is smaller than that for $C\underline{H}_3OH$ (57 and 78 kJ mol^{-1} ΔE^{TS}, respectively, at location 3 in $H_3PMo_{12}O_{40}$ cluster; Figure 2), because of the weaker C−H bonds at the carbonyl group. These results suggest that rate constants for secondary conversions of ethene via ODH routes can be smaller than those for its formation from ethane but that the opposite will be the case for methanol ODH to formaldehyde. Yet, measured selectivities to primary products are higher for methanol−O_2 reactions than ethane−O_2 reactions,[11] which suggests that reaction routes involving oxygen species other than lattice oxygens may be responsible for the combustion of the primary ethene products.[48]

Activation energies for C−H bonds in propane and in its primary propene product are shown in Figure 6c as a function of HAE. For the alkane, primary C−H bonds are stronger and have higher activation energy at each lattice O atom in a $H_3PMo_{12}O_{40}$ cluster ($(C\underline{H}_3)_2CH_2$, 443 kJ mol^{-1} BDE, 121 kJ mol^{-1} ΔE^{TS} at location 3 in $H_3PMo_{12}O_{40}$ cluster; Figure 2) than secondary C−H bonds ($(CH_3)_2C\underline{H}_2$, 427 kJ mol^{-1} BDE, 83 kJ mol^{-1} ΔE^{TS}). The allylic C−H bonds in propene are much weaker and thus exhibit lower activation energies (CH_2=$CHC\underline{H}_3$, 342 kJ mol^{-1} BDE, 72 kJ mol^{-1} ΔE^{TS}) than any of the C−H bonds in the alkane. In contrast, the bond strengths and activation energies of vinylic C−H bonds at terminal ($C\underline{H}_2$=$CHCH_3$, 480 kJ mol^{-1} BDE, 150 kJ mol^{-1} ΔE^{TS}) and methyl-substituted (CH_2=$C\underline{H}CH_3$, 458 kJ mol^{-1} BDE, 126 kJ mol^{-1} ΔE^{TS}) positions in propene are higher than for any of the C−H bonds in propane.

Figure 6d shows activation energies for C−H bonds in ethanol and in its primary ODH product (acetaldehyde) as a function of HAE. The C−H bonds in the methyl group of ethanol are stronger and exhibit higher activation energies at each O atom in $H_3PMo_{12}O_{40}$ clusters ($C\underline{H}_3CH_2OH$, 448 kJ mol^{-1} BDE, 121 kJ mol^{-1} ΔE^{TS}, at location 3 in $H_3PMo_{12}O_{40}$ cluster; Figure 2) than the C−H bonds adjacent to the OH group ($CH_3C\underline{H}_2OH$, 427 kJ mol^{-1} BDE, 83 kJ mol^{-1} ΔE^{TS}). The C−H bonds at the carbonyl position in acetaldehyde are much weaker and have lower activation energies ($CH_3C\underline{H}$=O, 385 kJ mol^{-1} BDE, 44 kJ mol^{-1} ΔE^{TS}) than any of the C−H bonds in ethanol. The strengths and activation energies of the C−H bonds allylic to the carbonyl group are slightly weaker than the C−H bonds at the same position in the parent alkanols, but such bonds have higher activation energies than at the corresponding methyl position in ethanol ($C\underline{H}_3CH$=O, 411 kJ mol^{-1} BDE, 143 kJ mol^{-1} ΔE^{TS}).

The dependences of activation energies on HAE and C−H BDE values are reflected in the slopes of the BEP relations shown in Figures 6 and 7, respectively; such slopes depend, in

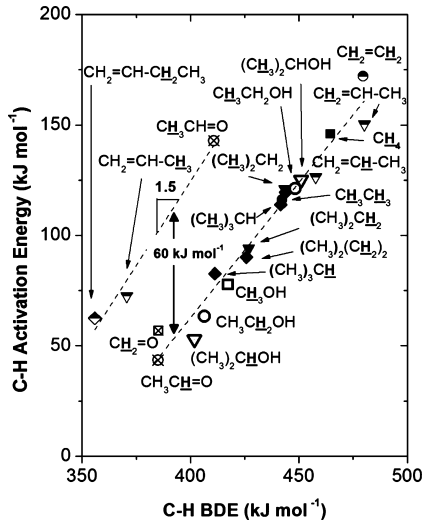

Figure 7. DFT-derived C−H bond activation energies in alkanes (closed symbols), alkanols (open symbols), alkenes (half-filled symbols), and alkanals (crossed symbols) at location 3 in $H_3PMo_{12}O_{40}$ clusters (Figure 2) as a function of their C−H bond dissociation energy (BDE).

turn, on the extent to which the C−H bond has cleaved and the O−H bond has formed at the transition state, as expected from the Hammond postulate.[30] Later transition states tend to resemble product states (in both structure and energy), which contain fully formed O−H bonds without any residual C−H bonds; as a result, activation energies will exhibit slopes with absolute values of unity with respect to both BDE and HAE. In contrast, early transition states resemble reactant states, thus leading to activation energies that are nearly insensitive to BDE or HAE, because C−H bonds will not have been cleaved and O−H bonds will not have been formed at such transition states.

The activation energy of the C−H bonds in $C\underline{H}_4$ depends strongly on HAE (slope 0.9; Figure 6a), suggesting that transition states contain nearly formed O−H bonds (Figure 5; $d_{O-H,TS}$ = 0.112 nm, $d_{O-H,prod}$ = 0.098 nm on $H_3PMo_{12}O_{40}$) and consequently C−H bonds that are nearly cleaved (Figure 5; $d_{C-H,TS}$ = 0.149 nm on $H_3PMo_{12}O_{40}$, $d_{C-H,react}$ = 0.110 nm). $C\underline{H}_3C\underline{H}_3$ and $(CH_3)_2C\underline{H}_2$ activation energies depend slightly

DOI: 10.1021/acs.jpcc.6b04604
J. Phys. Chem. C 2016, 120, 16741−16760

more weakly on HAE (slopes 0.82 each; Figure 6b,c), consistent with transition states with longer O−H bonds (Figure 5; $d_{O-H,TS}$ = 0.118−0. 122 nm, $d_{O-H,prod}$ = 0.098 nm) and shorter C−H bonds (Figure 5; $d_{C-H,TS}$ = 0.141−0.137 nm, $d_{C-H,react}$ = 0.110 nm) than those that mediate the activation of the stronger C−H bonds in CH_4. The transition states that cleave the weaker C−H bonds at alkanols also occur earlier along the reaction coordinate than for alkanes, as evident from their shorter C−H and longer O−H bonds than for the CH_4 activation transition state (Figure 5). These earlier transition states are less sensitive to the stability of the products formed, leading to smaller BEP slopes (vs HAE) than for the later transition states in CH_4 activation (e.g., 0.75 for $(CH_3)_2C\underline{H}OH$; 0.9 for $C\underline{H}_4$; Figure 6).

These BEP plots also show some curvature for stronger abstractors (more negative HAE), leading to smaller slopes for weaker bonds or stronger abstractors, because C−H activation events are less endothermic and lead to earlier transition states for such reactant−catalyst pairs.[30] These HAE effects can be described by the schematic representation of the Hammond's postulate shown in Scheme 3 in terms of transition states

Scheme 3. C−H Activation Transition State Energies Described in Terms of Overlaps between Potential Energy Surfaces for Dissociation of the C−H Bond and Formation of an O−H Bond at Metal Oxide Surface (MO*) and the Effect of Interaction Energy, E°_{int}, between Organic Radicals (R•, Formed by C−H Dissociation) and Hydroxylated Surface Oxygens (•MOH*, Formed by H-Addition to Oxide) on Lowering the Energy of Transition States at the Crossing Point of C−H and O−H Potentials

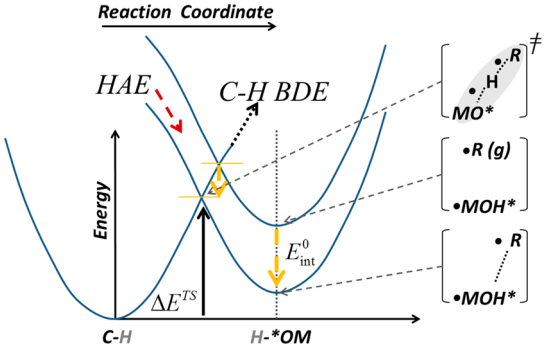

located at the crossing point of the C−H and O−H dissociation potentials. O−H potentials for lattice O atoms with more negative HAE will appear at a lower vertical position than those with less negative HAE; therefore, they will intersect a given C−H potential at a point closer to the equilibrium C−H bond distance, leading to earlier transition states along the reaction coordinate.

Figure 7 shows C−H activation energies in hydrocarbons and oxygenates as a function of C−H BDE at a given lattice O atom location in $H_3PMo_{12}O_{40}$ with a HAE value of −295 kJ mol^{-1} (shown by vertical dotted arrow in Figure 6). These C−H BDE effects exhibit two prominent deviations from expectations based on crossing C−H and O−H potentials (Scheme 3): (i) the regressed BEP slope (vs BDE) is greater than unity (∼1.3) for all C−H nonallylic bonds, and (ii) the activation energies for C−H bonds at allylic C atoms in propene, 1-butene, and acetaldehyde are larger (by 60 ± 10 kJ mol^{-1}) than predicted from their BDE values and the trends for nonallylic C−H bonds in alkanes and alkanols.

The strong sensitivity (slope ∼1.3) of C−H activation energies to C−H BDE for alkanes and alkanols (Figure 7) indicates that transition states for the activation of the stronger C−H bonds must overcome an energetic barrier even greater than that imposed by the energy differences among their C−H bonds. For instance, C−H bonds in $C\underline{H}_4$ are 22 and 63 kJ mol^{-1} stronger (Table 1) than those in $C\underline{H}_3C\underline{H}_3$ and $CH_3C\underline{H}OH$, respectively, yet C−H activation energies in $C\underline{H}_4$ are 30 and 93 kJ mol^{-1} larger than those in $C\underline{H}_3C\underline{H}_3$ and $CH_3C\underline{H}OH$. These DFT-derived energies and their sensitivity to C−H BDE are consistent with measured activation energies of CH_4 and C_2H_6, which differed more significantly than their respective C−H BDE values (activation energies 155 ± 9 kJ mol^{-1} for CH_4 and 110 ± 10 kJ mol^{-1} for C_2H_6 on O*-saturated Pt clusters).[49] The trends indicate that the rate constants for individual steps may depend on C−H bond energies more sensitively than anticipated, thus markedly disfavoring the retention of any desired intermediate products that contain weaker C−H bonds in sequential oxidation reactions and making attainable yields even lower than expected from BEP slopes (<1) (eq 3). Such effects reflect stronger interactions between the organic radicals and the hydroxylated surface O* at transition states that mediate the activation of a weaker C−H bond, as anticipated from measured activation energies[49] and confirmed below based on DFT-derived activation barriers.

The activation energies for allylic C−H bonds lie well above the BEP trends that describe the activation of other types of C−H bonds in hydrocarbons and oxygenates (Figure 7). For example, secondary C−H bonds in propane are 56 kJ mol^{-1} stronger than allylic C−H bonds in propene, but their activation energy is only 22 kJ mol^{-1} higher, instead of 73 kJ mol^{-1} (the value predicted from the BPE trends for nonallylic C−H bonds), than that for allylic C−H bonds in propene. As a result, the rate constants for these allylic C−H activation steps would differ much less than predicted by the BEP trends. At a temperature of 600 K, the $\exp(-(\Delta E^{TS}_{(CH_3)_2C\underline{H}_2} - \Delta E^{TS}_{CH_2=CH-C\underline{H}_3})/(RT))$ value relevant to the rate constant ratios for propane−propene sequential reactions ($\chi_1 = k_{ODH1}K_{ads1}/(k_{ODH2}K_{ads2})$; Scheme 1, eq 3) are 0.01 and 4.4 × 10^{-7}, respectively, for 22 and 73 kJ mol^{-1} activation energy differences. The calculated ratio of rate constants (χ_1), however, reflects a difference between ensemble averages of free energies (ΔG^{TS}) of all C−H bonds contributing to activation of each molecule. We show in section 3.6, that χ_1 derived from such ensemble averages at an O atom in $H_3PMo_{12}O_{40}$ cluster (at location 3 in Figure 2) has a value near 0.1 for propane−propene reactions at 600 K, in excellent agreement with rate ratio of 0.2 measured at 600 K on supported VO_x/SiO_2 catalysts.[15] These results suggest that the deviations from BEP trends for allylic bonds decrease the rate constant for secondary reactions in propene, leading to higher propene yields than expected in the absence of such radical pair interactions.

These deviations in DFT-derived activation energies from the monotonic trends with C−H BDE suggest that both BDE and HAE are relevant but incomplete descriptors of reactivity for general classes of molecules that react via H-abstraction on oxide surfaces. We surmise, based on Born−Haber cycle formalisms discussed above and described in Scheme 2, that

DOI: 10.1021/acs.jpcc.6b04604
J. Phys. Chem. C 2016, 120, 16741−16760

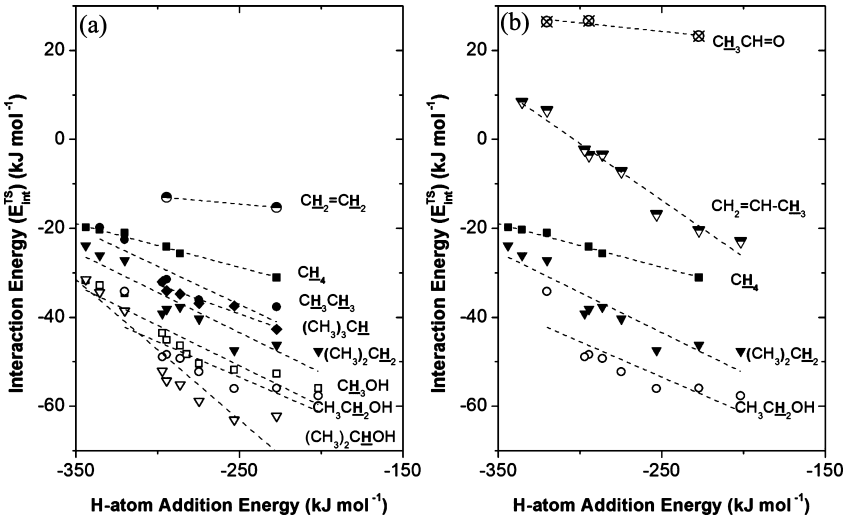

Figure 8. Interaction energies between organic radicals (R•, Scheme 2) and hydroxylated metal oxide species (•MOH*, Scheme 2) at transition states (E_{int}^{TS}, eq 5) for C−H activation in (a) weakest C−H bonds in alkanes (closed symbols), alkanols (open symbols), and alkenes (half-open symbols), and (b) C_3H_8, C_2H_5OH, and the allylic C−H bonds in their primary products, as a function of H-atom addition energy (HAE) on POM clusters. Dashed lines represent regressed linear fits to E_{int}^{TS} trends.

such deviations reflect interactions between the organic radicals and the hydroxylated oxide surface at the transition state and the product state; such interactions depend on properties of molecules and H-abstractors that are not uniquely described by their respective C−H BDE and HAE values, thus making scaling relations incomplete and inaccurate as predictors of reactivity and selectivity.

3.5. Radical−Surface Interactions and More Complete Descriptors of Reactivity in Oxidation Reactions Involving Hydrogen Abstraction Events. *3.5.1. Interactions between Unpaired Electrons at Organic Radicals and Hydroxylated Metal Oxide Surface.* Born−Haber thermochemical cycles (Scheme 2) dissect transition state energies and activation barriers for C−H activation (ΔE^{TS}) into C−H BDE, HAE at lattice O atoms, and the interaction energy between the organic radicals and the hydroxylated oxygen species at the transition state (E_{int}^{TS}; eq 5). These E_{int}^{TS} values cannot be obtained directly but can be estimated by subtracting the DFT-derived C−H BDE (Table 1) and HAE (Table 2) values from ΔE^{TS} values (Figure 6). These E_{int}^{TS} values for C−H activation transition states are shown as a function of HAE in Figure 8. The negative E_{int}^{TS} values reflect radical−surface interactions that significantly stabilize transition states. For alkanes and alkanols, these interactions (at each HAE) become more negative for more substituted C atoms, which also exhibit smaller values of C−H BDE (Figure 8a). These effects of weaker C−H bonds, combined with the tendency of the radicals that they form to interact more strongly with surface O−H species, combine to give the larger than unity slopes observed for the effects of C−H BDE on activation energies (Figure 7). For each given HAE value, allylic C−H bonds in propene, 1-butene, and acetaldehyde showed much less negative E_{int}^{TS} values than those in alkanes and alkanols (Figure 8b), because organic radicals formed by dissociating these C−H bonds interact less strongly with surface OH radicals than the radicals formed from the saturated reactants. These weaker interactions dampen the expected benefits of their weaker C−H bonds on ΔE^{TS}, leading to activation energies that lie above the trend lines observed for saturated reactants (Figure 7).

The interaction energies (E_{int}^{TS} values) shown in Figure 8 can be described by the expected attractive interactions between unpaired electrons at the p-orbitals in organic radicals (R•, Scheme 2) and those at d-orbitals in the metal centers bound to the hydroxylated lattice oxygens (•MOH*, Scheme 2). Such unpaired electron pairs act as molecular magnets; their interactions determine the structure and stability of organic and organometallic diradical complexes and the arrangement of diradical molecules within liquid crystals, as shown by theory and experiment.[50−52] We examine next how these radical-surface interactions are influenced by the extent to which radicals have formed at different transition states and with the molecular identity of the organic radicals involved.

Radical−surface interactions become weaker (less negative E_{int}^{TS}) at all transition states when lattice oxygens have stronger H-abstraction strengths (more negative HAE) (Figure 8). These weaker interactions coincide with the incomplete formation of the organic radicals and of the surface O−H bonds for transition states that occur earlier along the reaction coordinate for more exothermic reactions. In contrast, weaker H-abstractors activate C−H bonds via product-like transition states with fully formed radical pairs that interact most strongly. The values of E_{int}^{TS} reflect the extent to which these radical pairs have already fully formed at the transition state, thus asymptotically approaching the interaction energies present at the product state (E_{int}°) for weak H-abstractors and strong C−H bonds.

The values of E_{int}° in the products formed in C−H activation elementary steps depend on the location and distribution of their unpaired electron in the organic and inorganic moieties at the product state. The different electron distributions in the products of C−H bond activation in propane ($(CH_3)_2C\underline{H}_2$) and propene (CH_2=$C\underline{H}CH_3$) are illustrated in Figure 9, which show DFT-derived spin-density maps of the two unpaired electrons at the triplet state products formed in these two reactions on $H_3PMo_{12}O_{40}$ cluster (at location 3 shown in Figure 2). These electrons occupy a p-orbital in the organic radicals and a d-orbital at a metal center in the POM cluster. The propane-derived organic radical shows the electron highly localized at the secondary C atom from which the H atom was

DOI: 10.1021/acs.jpcc.6b04604
J. Phys. Chem. C 2016, 120, 16741−16760

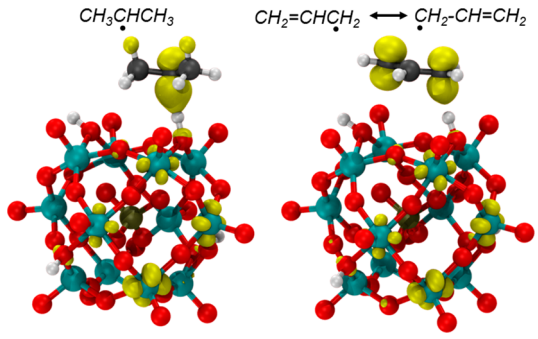

Figure 9. Spin-density maps depicted by yellow surfaces at 50 e nm^{-3}, representing the location of unpaired radical electrons in isopropyl and propene allyl radicals interacting with hydroxylated O atom at location 3 in $H_3PMo_{12}O_{40}$ cluster (Figure 2) derived from fully relaxed triplet DFT calculations. The maps represent one d-electron and a total of two electrons.

removed. In contrast, the unpaired electron in propene-derived radicals is delocalized through allylic resonance structures (CH_2═CH−$CH_2^{\bullet}$ ←→ $^{\bullet}CH_2$−CH═CH_2; Figure 9). The delocalized nature of unpaired electrons in allylic organic radicals leads, in turn, to weaker diradical interactions than when unpaired electrons remain localized at the C atom from which the H atom was abstracted (Figure 8). It is precisely such delocalization, in fact, that causes C−H BDE values to be smaller for C−H bond activation at allylic positions than at other positions and in parent alkanes.

3.5.2. Relating Interaction Energies in Product States to Those at the Relevant Transition States. The individual components of the interaction energies at the transition states (E_{int}^{TS}) cannot be rigorously extracted from its DFT-derived total energy, but it can inferred from that in the product state (E_{int}°) using the formalism of crossing potential models;[14] in this case, these are the potentials for C−H cleavage and O−H formation; the energies at their crossing point determine the location of the transition state along the reaction coordinate. As shown in Scheme 3, when radicals and surface hydroxyls have a favorable (i.e., negative) interaction energy in the product state (E_{int}°), the O−H formation potential appears at a lower point in the ordinate than for noninteracting radicals, thus crossing the C−H dissociation potential curve at a lower energy than for noninteracting systems. As C−H and O−H bond lengths vary along the reaction coordinate, their energies can be described approximately by harmonic potentials of similar curvature (Scheme 4), even though their bond vibrational frequencies differ slightly ($\nu_{C-H} \approx 3100$ cm^{-1}, $\nu_{O-H} \approx 3700$ cm^{-1}). In such formalisms, the C−H activation transition state then lies at the crossing point of these two potentials and its energy (ΔE^{TS}) is given by[14]

$$\Delta E^{TS} = \frac{(\lambda + \Delta E^{\circ})^2}{4\lambda} \quad (6)$$

where ΔE° is the overall step energy, given by the sum of C−H BDE, HAE, and the radical−surface interaction energy at the product state,

$$\Delta E^{\circ} = \mathrm{BDE} + \mathrm{HAE} + E_{int}^{\circ} \quad (7)$$

and λ represents the energy of the harmonic O−H potential at the minimum energy point of the C−H potential curve. The sensitivity of the interaction energy at the transition state

Scheme 4. Crossing Harmonic Potential Model Used To Describe the Effects of Reactant and Product Bond-Strengths and Radical−Surface Interactions on C−H Activation Energies[a]

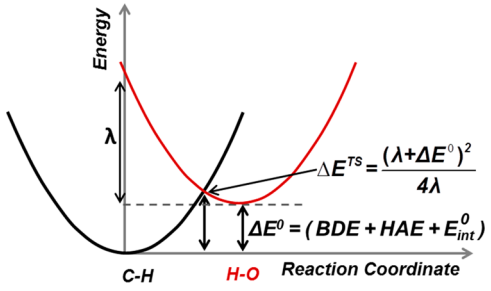

[a]The relation between activation energies represented by the crossing point of C−H and O−H potentials (ΔE^{TS}) and the reaction energies (ΔE°) are given by eq 6.

(ΔE^{TS}) to that at the product state (ΔE°) is then given by the derivative of ΔE^{TS} with respect to ΔE°:

$$\frac{d\Delta E^{TS}}{d\Delta E^{\circ}} = \frac{1}{2} + \frac{\Delta E^{\circ}}{2\lambda} \quad (8)$$

As reaction energies (ΔE°) increase and approach $+\lambda$ for very endothermic reactions, the slope approaches unity (eq 8) and activation energies equal the reaction energies ($\Delta E^{TS} = \Delta E^{\circ} = +\lambda$, eq 6), consistent with the very late character of the transition states involved. As ΔE° values approach $-\lambda$ for very exothermic reactions, activation barriers become independent of ΔE° (zero slope, eq 8) and asymptotically approach zero ($\Delta E^{TS} = 0$, eq 8), as expected for very early transition states. ΔE° values above $+\lambda$ would cause the slopes of ΔE^{TS} vs ΔE° to become larger than unity, while those more negative than $-\lambda$ would actually lead to an increase in ΔE^{TS} as reactions become less exothermic. Such anomalous effects for extreme reaction thermodynamics are physically possible but very rarely observed.[53] All DFT-derived activation energies exhibit slopes between 0 and 1 with respect to HAE (Figure 6), consistent with reaction energies between $-\lambda$ and $+\lambda$ for the oxidation reactions and H-abstractors of interest.

The difference in interaction energies between incipiently formed organic radicals and surface hydroxyls at the transition state (E_{int}^{TS}) and their fully formed analogs in product state (E_{int}°) is given by combining eqs 5−7:

$$E_{int}^{TS} - E_{int}^{\circ} = \frac{(\lambda - \Delta E^{\circ})^2}{4\lambda} \quad (9)$$

This equation can be rearranged to define a parameter η that characterizes the "lateness" of the transition state:

$$\eta = 1 - \frac{E_{int}^{TS} - E_{int}^{\circ}}{\lambda} = 1 - \left(\frac{\lambda - \Delta E^{\circ}}{2\lambda}\right)^2 \quad (10)$$

which ranges from 0 to 1 for reaction energies (ΔE°) of $-\lambda$ and $+\lambda$, respectively. Next, we use these crossing potential constructs to describe how DFT-derived C−H activation transition state energies depend on reaction energies and how η varies among transition states in oxidation reactions limited by H-abstraction elementary steps. This is done by a regression of the values of ΔE^{TS}, E_{int}°, and λ to the functional form of eq 6 and the subsequent determination of η for each transition state using eqs 7 and 10.

DOI: 10.1021/acs.jpcc.6b04604
J. Phys. Chem. C 2016, 120, 16741−16760

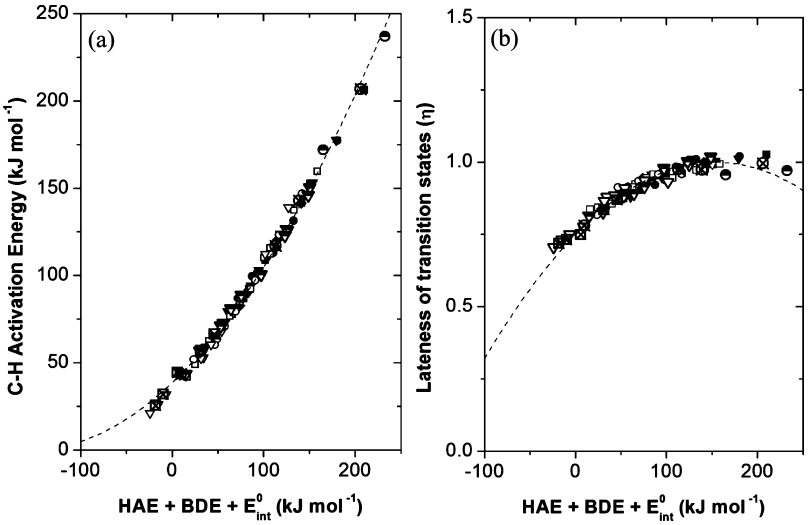

Figure 10. (a) DFT-derived C−H bond activation energies and (b) a dimensionless parameter η representing lateness of the transition state as defined by eq 10 in alkanes (closed symbols), alkanols (open symbols), alkenes (half-filled symbols), and alkanals (crossed symbols), as a function of the sum of the C−H BDE of reactants, the HAE of abstractors, and the product state interaction energy (E°_{int}). Dashed curves represent regressed values of the activation energies to the functional form of eqs 6 (panel a) and 10 (panel b).

Table 3. Diradical Interaction Energy between Organic Radicals Formed as Products of C−H Bond Activation and the Hydroxylated MO* Surface Species

molecule	C−H Bond	regressed E°_{int} values[a] (kJ mol^{-1})	DFT-derived E°_{int} on $H_3PMo_{12}O_{40}$[b] (kJ mol^{-1})	DFT-derived E°_{int} on $H_3PW_{12}O_{40}$[b] (kJ mol^{-1})
CH_4	CH_4	−27 ± 1	−25	−22
C_2H_6	CH_3CH_3	−35 ± 2	−37	−37
C_3H_8	$CH_3CH_2CH_3$	−46 ± 1	−48	−45
	$CH_3CH_2CH_3$	−30 ± 4		
i-C_4H_{10}	$(CH_3)_2CHCH_3$	−43 ± 2	−55	−45
	$(CH_3)_2CHCH_3$	−32 ± 4		
n-C_4H_{10}	$CH_3CH_2CH_2CH_3$	−50 ± 5		
	$CH_3CH_2CH_2CH_3$	−36 ± 4		
CH_3OH	CH_3OH	−57 ± 2	−49	−46
C_2H_5OH	CH_3CH_2OH	−62 ± 2	−81	−51
	CH_3CH_2OH	−35 ± 4		
C_3H_7OH	$(CH_3)_2CHOH$	−73 ± 2	−117	−71
	$(CH_3)_2CHOH$	−33 ± 4		
C_2H_4	$CH_2{=}CH_2$	−20 ± 2		
C_3H_6	$CH_2{=}CHCH_3$	−35 ± 4		
	$CH_2{=}CHCH_3$	−38 ± 4		
	$CH_2{=}CHCH_3$	−20 ± 2	−31	−25
1-C_4H_8	$CH_2{=}CHCH_2CH_3$	−15 ± 3		
CH_2O	$CH_2{=}O$	−59 ± 3	−34	−30
CH_3CHO	$CH_3CH{=}O$	−81 ± 7		
	$CH_3CH{=}O$	23 ± 2	−11	−11

[a]Derived from regression of activation energies to the form of eq 6; regressed λ = 154 ± 4 kJ mol^{-1}; uncertainties represent 95% confidence intervals [b]Derived from difference between DFT energies of noninteracting and interacting radicals (eq 11).

C−H activation energies (ΔE^{TS}) for all reactants are shown in Figure 10a as a function of the reaction energy (ΔE° = BDE + HAE + E°_{int}). A value of E°_{int} was obtained for each C−H bond in each alkane, alkanol, alkene, and alkanal reactant by regressing the C−H activation energies (Figure 6) to the form of eq 6 over the full HAE range of O atoms exposed at POM cluster surfaces (−356 to −196 kJ mol^{-1}; Table 2); C−H BDE (Table 1) and HAE (Table 2) values represent properties unique to each reactant and abstractor, respectively. We first consider a single value of λ parameter in eq 6 for all C−H bonds and surface oxygens and let E°_{int} values vary only with the identity of the reactant C−H bond but not with the properties of the H-abstractor. We then assess the uncertainties in the regressed values and their ability to accurately describe DFT-derived values of E°_{int} without additional assumptions or parameters.

The dashed curve drawn through the points in Figure 10a represents the regressed best fit of all DFT-derived activation energies to the form of eq 6 with a single λ value and with E°_{int} values that vary only with the identity of the C−H bond. The local slopes shown by the points and the regression decrease as C−H activation steps become more favored by thermody-

DOI: 10.1021/acs.jpcc.6b04604
J. Phys. Chem. C 2016, 120, 16741−16760

namics (ΔE° values decrease and become negative), consistent with earlier transition states that become less sensitive to the stability of the product state, as predicted from eq 8. The regressed λ value (154 ± 4 kJ mol^{-1}; ±95% confidence interval) and the E°_{int} values for each different type of C−H bond in each of the alkane, alkene, alkanol, and alkanal molecules are shown in Table 3. These E°_{int} values become more negative for more substituted C atoms in alkanes and alkanols (−27 ± 1 kJ mol^{-1} for C$\underline{H}_4$ to −73 ± 2 kJ mol^{-1} for $(CH_3)_2C\underline{H}OH$) and less negative for allylic C−H bonds than bonds in saturated reactants (−20 ± 2 kJ mol^{-1} for $C\underline{H}_3CH{=}CH_2$), consistent with the observed trends in DFT-derived activation energies with C−H bond substitution. The lateness parameter (η), calculated for each transition state using these regressed values and eq 10 is shown as a function of reaction energy (ΔE°) in Figure 10b. These η values are near unity for most transition states, decreasing to ∼0.7 only for the most negative ΔE° values (−24 kJ mol^{-1} for $(CH_3)_2C\underline{H}OH$ activation on $H_3PMo_{12}O_{40}$ cluster with DFT+U treatment; U = 8 eV) among the C−H bonds and abstractors examined.

The activation energies and η values are single-valued functions of ΔE° (Figure 10), indicating that the E°_{int} value for all C−H bonds in alkanes, alkenes, alkanols, and alkanals is sufficient to account for interaction energies for all abstractors, even though the HAE values of these abstractors significantly influence the lateness of the transition states. Thus, these E°_{int} values, in the context of crossing-potential constructs, accurately bring together the apparently disparate effects of HAE and BDE on activation energies for different C−H bonds (Figures 6 and 7) and, in doing so, provide a much more complete, useful, and rigorous descriptor than those provided by linear BEP relations with HAE and BDE. The DFT-derived activation energies as a function of reaction energies (ΔE°) (Figure 10) show some slight deviations (±5 kJ mol^{-1}) and only at very high and low ΔE° values from the regressed curve and from the functional form of eq 6. These deviations reflect small changes in λ (eq 6) with reactants or the product state diradical interaction energies (E°_{int}) with abstractor strengths. The strong effects of the C−H bond identity and of the H-abstractor on E^{TS}_{int} values (Figure 8) and their consequences for activation energies (Figures 6 and 7) are, however, accurately captured by descriptors (eq 6, ΔE° = BDE + HAE + E°_{int}) that assume a single constant λ value for all molecules and abstractor and abstractor-independent E°_{int} values.

Next, we examine the small effects of abstractor strength on E°_{int} by comparing their regressed values with DFT-derived interaction energies between isolated radicals (R$^\bullet$) and hydroxylated POM clusters ($^\bullet$MOH*, Scheme 3). Radical−surface interaction energies at the product state ($E^\circ_{int,DFT}$) were determined from the difference between DFT-derived energies for interacting radicals at the product state ($E_{R^\bullet\cdots HOM^\bullet}$, Scheme 2) and for the respective isolated species ($E_{R^\bullet}$, $E_{HOM^\bullet}$):

$$E^\circ_{int,DFT} = E_{R^\bullet\cdots HOM^\bullet} - E_{R^\bullet} - E_{HOM^\bullet} \quad (11)$$

These $E^\circ_{int,DFT}$ values for an O atom at location 3 (Figure 2) in $H_3PMo_{12}O_{40}$ and $H_3PW_{12}O_{40}$ clusters (−295 and −227 kJ mol^{-1} HAE, respectively; Table 2) and the corresponding E°_{int} values regressed from DFT-derived activation energies (to the form of eq 6) for organic radicals derived from C−H activation in alkanes, alkenes, alkanols, and alkanals are shown in Table 3.

The $E^\circ_{int,DFT}$ values of radicals formed from activation of C−H bonds at terminal C atoms in all molecules, allylic C−H bonds in alkenes and alkanals, and the secondary C atom in $(CH_3)_2C\underline{H}_2$ in $H_3PMo_{12}O_{40}$ (location 3, Figure 2) are similar (within ±5 kJ mol^{-1}, Table 3) to those in $H_3PW_{12}O_{40}$, even though $E^\circ_{int,DFT}$ values vary from −10 to −50 kJ mol^{-1} with C−H bond identity in a given cluster. These similar interaction energies for a given radical on O atoms with very different HAE values (−295 and −227 kJ mol^{-1} on $H_3PMo_{12}O_{40}$ and $H_3PMo_{12}O_{40}$, respectively; Table 2) are consistent with diradical interactions that depend only weakly on the abstractor strength (HAE). In contrast with these weakly interacting radicals ($E^\circ_{int,DFT}$ values between −10 to −50 kJ mol^{-1}; Table 3), the $E^\circ_{int,DFT}$ values for radicals derived from $(CH_3)_3C\underline{H}$, $CH_3C\underline{H}_2OH$, and $(CH_3)_2C\underline{H}OH$ were more negative on $H_3PMo_{12}O_{40}$ clusters ($E^\circ_{int,DFT}$ values between −55 to −117 kJ mol^{-1}) than on $H_3PW_{12}O_{40}$ ($E^\circ_{int,DFT}$ values between −45 to −71 kJ mol^{-1}), and their regressed E°_{int} values are intermediate between the DFT-derived values for each of two abstractors. Thus, assumptions of crossing potentials with abstractor independent product state diradical interactions provide accurate correction to deviations from monotonic effects of HAE and BDE and provide more complete descriptors of C−H activation reactivity, but such assumptions become less accurate for strongly interacting radicals.

We conclude that diradical interactions at transition states are essential to describe reactivity and selectivity in oxidation reactions involving H-abstraction steps and, by inference, for general classes of reactions involving homolytic-type bond cleavage steps and transition states with significant radical character. These interactions must be taken into account in using BEP-type scaling relations that rely solely on C−H BDE values for reactants and HAE values for H-abstractors; these provide useful but incomplete descriptions of reactivity for oxides and other H-abstractors in oxidations of organic substrates.

3.6. Role of Hydrogen Abstractor Strengths and Reaction Temperatures in Determining Practical Attainable Product Selectivities and Yields in Sequential Oxidation Reactions. As C−H activation steps become more exothermic on surface O atoms that form stronger OH bonds in product states (i.e., ΔE° = BDE + HAE + E°_{int} values decreases with more negative HAE), their transition states occur earlier along the reaction coordinate (eq 10) and activation barriers become less sensitive to BDE, HAE, and E°_{int} values (eq 8). The consequently weaker effects of reaction thermodynamics on activation barriers dampens the effects of C−H bond energies for stronger H-abstractors.

Next, we examine the effects of abstractor strength on some illustrative examples of sequential ODH reactions of alkanes and alkanols to form alkenes and alkanals, respectively. Except for the ethane−ethene pair, these reactions involve initial products with C−H bonds weaker than those in reactants. The difference between activation energies for each reactant−product pair, methane−ethane ($\Delta E^{TS}_{C\underline{H}_4} - \Delta E^{TS}_{C\underline{H}_3C\underline{H}_3}$), propane−propene ($\Delta E^{TS}_{(CH_3)_2C\underline{H}} - \Delta E^{TS}_{C\underline{H}_3CH=CH_2}$), methanol−formaldehyde ($\Delta E^{TS}_{C\underline{H}_3OH} - \Delta E^{TS}_{C\underline{H}_2=O}$), ethane−ethene ($\Delta E^{TS}_{C\underline{H}_2=C\underline{H}_2} - \Delta E^{TS}_{C\underline{H}_3C\underline{H}_3}$), and methane−formaldehyde ($\Delta E^{TS}_{C\underline{H}_4} - \Delta E^{TS}_{C\underline{H}_2=O}$), are shown in Figure 11 for H-abstractors with a very broad HAE range (−527 to −196 kJ mol^{-1}); these abstractors include O atoms of POM clusters and even gaseous CH_3 and OH radicals. The activation energy differences shown in Figure 11 determine the ratio of rate constants for the respective activation of reactants and initial products (as described by eqs 3 and 4); their values determine maximum attainable yields

DOI: 10.1021/acs.jpcc.6b04604
J. Phys. Chem. C 2016, 120, 16741−16760

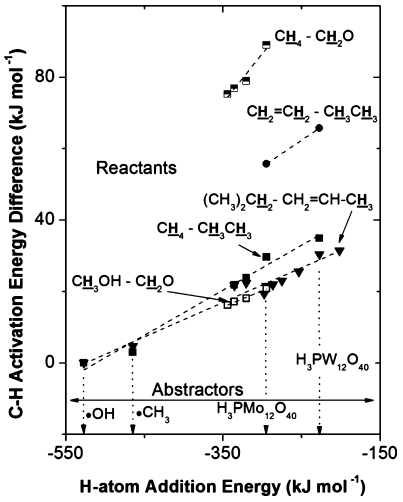

Figure 11. DFT-derived activation energy differences between reactants and primary products as a function of HAE of POM clusters and methyl and hydroxyl radicals as H-abstractors. These activation energy differences represent ratios of rate constants for activation of reactants and primary products (eqs 3 and 4), which ultimately determined maximum attainable yields to primary products in sequential oxidative dehydrogenation routes (Scheme 1).

of primary products as conversion increases in these sequential oxidation reactions (Scheme 1).

In the case of propane–propene pairs, secondary C–H bonds in propane are stronger than allylic C–H bonds in propene (by 56 kJ mol^{-1}; Table 1), but the product state diradical interactions (E°_{int}) are also stronger in propane than propene C–H activation steps (by 23 kJ mol^{-1}; Table 3), leading to a difference of 33 kJ mol^{-1} in their product state energies (BDE + E°_{int}) for a given H-abstractor. On weak H-abstractors (e.g., an O atom in a $H_3PW_{12}O_{40}$ with −227 kJ mol^{-1} HAE), the difference in activation barriers between propane and propene (31 kJ mol^{-1}) is nearly the same as the difference in their respective reaction energies (33 kJ mol^{-1}), as expected from the lateness of their transition states. These activation barriers become similar as HAE values become more negative, because reactant-like transition states cannot sense the strength of the C–H bonds being cleaved. CH_3 and OH radicals are very strong H-abstractors (HAE = −464 and −527 kJ mol^{-1}) because they form stable CH_4 and H_2O molecules; they lead to activation energies for propane and propene that differ by less than 5 kJ mol^{-1} (Figure 11). Similar trends are evident for other reactant–product pairs (Figure 11); in all cases, weak and strong C–H bonds cleave with activation energies that become similar as abstractors become stronger, as previously concluded from kinetic and isotopic data for oxidative CH_4 coupling reactions.[16,54]

Higher temperatures dampen differences in rate constants among molecules for a given H-abstractor (eqs 3 and 4). The activation free energy differences (ΔG^{TS}) that determine the ratios of rate constants for C–H activation in reactants and products (e.g., χ_1 for alkane–alkene, eq 3) include contributions from activation enthalpies (ΔH^{TS}) and entropies (ΔS^{TS}):

$$\chi_1 = e^{-\Delta\Delta G^{TS}/(RT)} = e^{-(\Delta\Delta H^{TS} - T\Delta\Delta S^{TS})/(RT)} = e^{\Delta\Delta S^{TS}/R}\, e^{-\Delta\Delta H^{TS}/(RT)} \quad (12)$$

Higher activation enthalpies in reactants with C–H bonds stronger than in primary products and modest reaction temperatures lead to $\exp(-\Delta\Delta H^{TS}/(RT))$ values and rate ratios (χ_1) much lower than unity. These enthalpy differences become less consequential as temperature increases, leading to

Table 4. Degeneracy of Different C–H Bonds (n_i) in Alkanes, Alkanols, Alkenes, and Alkanals and Their DFT-Derived Electronic Energies (ΔE^{TS}), Enthalpies (ΔH^{TS}), and Entropies (ΔS^{TS}) of Activation at Location 3 in $H_3PMo_{12}O_{40}$ Cluster (Figure 2)

molecule	C–H bond	n_i	ΔE^{TS},[a] kJ mol^{-1}	ΔH^{TS},[b] kJ mol^{-1}	ΔS^{TS},[b] J mol^{-1} K^{-1}
CH_4	CH_4	4	146	128	−100
C_2H_6	CH_3CH_3	6	116	97	−109
C_3H_8	$CH_3CH_2CH_3$	2	94	74	−117
	$CH_3CH_2CH_3$	6	124	107	−107
i-C_4H_{10}	$(CH_3)_2CHCH_3$	1	83	64	−118
	$(CH_3)_2CHCH_3$	9	120	100	−107
n-C_4H_{10}	$CH_3CH_2CH_2CH_3$	4	90	68	−93
	$CH_3CH_2CH_2CH_3$	6	114	92	−91
CH_3OH	CH_3OH	3	78	61	−121
C_2H_5OH	CH_3CH_2OH	2	63	47	−126
	CH_3CH_2OH	3	121	103	−107
C_3H_7OH	$(CH_3)_2CHOH$	1	53	37	−127
	$(CH_3)_2CHOH$	6	118	101	−107
C_2H_4	$CH_2=CH_2$	4	172	128	−188
C_3H_6	$CH_2=CHCH_3$	2	150	107	−188
	$CH_2=CHCH_3$	1	126	72	−190
	$CH_2=CHCH_3$	3	72	56	−132
1-C_4H_8	$CH_2=CHCH_2CH_3$	1	63	46	−132
CH_2O	$CH_2=O$	2	57	44	−130
CH_3CHO	$CH_3CH=O$	1	43	31	−130
	$CH_3CH=O$	3	144	127	−107

[a]Calculated at 0 K, vacuum. [b]Determined at 298.15 K and 101.325 kPa (see Supporting Information).

DOI: 10.1021/acs.jpcc.6b04604
J. Phys. Chem. C 2016, 120, 16741–16760

ratios of rate constants that depend solely on differences in activation entropies.

The weaker effects of activation enthalpy differences to these rate ratios at higher temperatures cause the less preferential activation of weakest C−H bonds as temperature increases to those required for practical catalysis, dampening to some extent differences in reactivity among molecules.[15] The rate constant ($k_{ODH}K_1$) for C−H activation in a given molecule reflects the ensemble-averaged reactivity of each of its C−H bonds:[15]

$$k_{ODH}K_{ads} \approx \sum_i n_i \, e^{\Delta S_i^{TS}/R} \, e^{-\Delta H_i^{TS}/(RT)} = e^{\langle \Delta S^{TS} \rangle / R} \, e^{-\langle \Delta H^{TS} \rangle / (RT)} \quad (13)$$

Here, η_i is the number of C−H bonds of a given type within a molecule and ΔH_i^{TS} and ΔS_i^{TS} are their enthalpies and entropies of activation. $\langle \Delta H^{TS} \rangle$ and $\langle \Delta S^{TS} \rangle$ represent ensemble averages of these respective thermodynamic quantities over all C−H bonds in a given molecule. In such cases, the ratios of rate constants described in eq 12 must also include ensemble averaged activation enthalpy and entropy differences:

$$\chi_1 = e^{\Delta \langle \Delta S^{TS} \rangle / R} \, e^{-\Delta \langle \Delta H^{TS} \rangle / (RT)} \quad (14)$$

Such averaging, inaccessible in experiments, can be rigorously implemented using DFT-derived activation energies and entropies for each C−H bond within each molecule examined in this study.

Next, we examine how reaction temperatures and ensemble-averaged C−H activation enthalpy and entropy differences influence the ratios of rate constants for specific pairs of reactants and primary products involved in sequential C−H activation reactions. The η_i, ΔH_i^{TS}, and ΔS_i^{TS} values required for these examinations are shown in Table 4.

Figure 12 shows ratios of rate constants (χ values in eq 14) for methane−ethane, propane−propene, methanol−formaldehyde, ethanol−acetaldehyde, and ethane−ethene sequential C−H activation reactions on $H_3PMo_{12}O_{40}$ clusters (at location 3 in Figure 2) as a function of reciprocal temperatures. The χ values for methane−ethane, propane−propene, and ethane−ethene reactions at the same O atom location in $H_3PW_{12}O_{40}$ clusters are also shown in Figure 12 to contrast abstractors with different HAE values (−295 and −227 kJ mol^{-1} here the HAE values). At modest temperatures (400 K, Figure 12), all χ values are much smaller than unity because (i) enthalpy differences contribute significantly to rate ratios, (ii) ensemble-averaged enthalpy values are dominated by the weakest C−H bond in each pair, and (iii) the weakest C−H bonds in the reactants (numerator terms in eqs 3, and 4) are much stronger than those in the primary products (denominator terms in eqs 3 and 4). The differences in ensemble-averaged enthalpies between reactants and products become smaller as temperatures increase, and the ratios of rate constants ultimately approach values given by the corresponding differences in ensemble averaged activation entropies (eq 13). For example, the χ_1 value for propane−propene sequential reactions is 0.01 at 400 K (Figure 12), because of the large differences in activation enthalpies between the methylene C−H bond in propane and the allylic C−H bond in propene ($\Delta H^{TS}_{(CH_3)_2C\underline{H}} - \Delta H^{TS}_{\underline{CH}_3CH=CH_2}$ = +18 kJ mol^{-1}, Table 4); this ratio, however, actually becomes larger than unity above 1200 K, because activation entropies favor reactions of C−H bonds in propane ($\Delta S^{TS}_{(CH_3)_2C\underline{H}} - \Delta S^{TS}_{\underline{CH}_3CH=CH_2}$ = +16 J mol^{-1} K^{-1}, $\Delta S^{TS}_{(C\underline{H}_3)_2CH} - \Delta S^{TS}_{CH_3C\underline{H}=CH_2}$ = +83 J mol^{-1} K^{-1}, Table 4). These χ_1 values are 0.07−0.17 at temperatures typical of propane ODH reactions (550−700 K). In a similar manner, χ values larger than unity are reached for methanol−formaldehyde, ethanol−acetaldehyde, and methane−ethane reactions at sufficiently high temperatures (Figure 12).

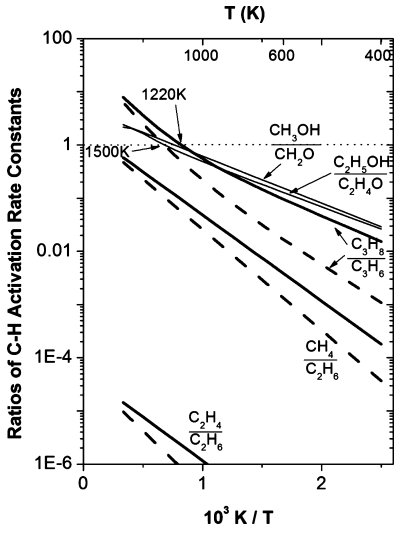

Figure 12. Ratios of rate constants for activation of the reactant organic molecules and for activation of the desired primary products formed from them on $H_3PMo_{12}O_{40}$ (solid lines) and $H_3PW_{12}O_{40}$ (dashed lines) clusters as a function of reciprocal temperature. The rate constants represent ensemble-averaged rate constants for all C−H bonds in a given molecule using the activation energies and degeneracies shown in Table 4.

At any given temperature, χ values for these sequential reactions are larger on stronger abstractors ($H_3PMo_{12}O_{40}$; location 3, −295 kJ mol^{-1} HAE; Table 2) than on weaker ones ($H_3PW_{12}O_{40}$; location 3, −227 kJ mol^{-1} HAE; Table 2) (Figure 12) because stronger abstractors cleave C−H bonds at earlier transition states, which are less sensitive to C−H and lead to smaller activation enthalpy differences among C−H bonds with different BDE values (Figure 11). Thus, stronger abstractors and higher temperatures dampen the kinetic effects of differences in C−H bond energies and lead to higher selectivities and yields of intermediate products with weaker C−H bonds than in the reactants from which they form.

These illustrative examples, chosen because of their representative and practical nature in catalytic oxidations of hydrocarbons and oxygenates, show how yields and selectivities to primary products depend on the activation free energies of the C−H bonds involved. Their different C−H BDE values influence activation enthalpies less strongly at high temperatures and on strong abstractors, thus decreasing the otherwise ubiquitous preference for activating the weakest C−H bonds in molecules. Such trends are at odds with the frequent guidance to improve selectivities by using softer oxidants and lower temperatures, a strategy that is, in any case, self-contradictory, given the lower reactivity of weaker H-abstractors. The effects of C−H BDE and HAE on reactivity are also perturbed by diradical interactions between organic and OH radicals at C−H activation transition states; these interactions must be included in defining accurate descriptors of reactivity for these types of reactions, which cannot be solely based on BEP-type scaling relations. These diradical-type interactions, previously ne-

DOI: 10.1021/acs.jpcc.6b04604
J. Phys. Chem. C 2016, 120, 16741−16760

glected as descriptors of reactivity in catalytic oxidations, may expand the narrow yield limits espoused based on such linear free energy scaling relations, but only through the design of catalytic solids with H-abstractors that preferentially destabilize allylic radicals at transition states relative to those formed via H-abstraction from saturated reactants. The analyses presented here are applicable to homolytic C−H bond cleavage prevalent in most selective oxidation catalysts that have octahedral metal−oxygen coordination. Metal centers in other oxides with fewer O atom neighbors may be directly accessible to reactants, leading to heterolytic C−H cleavage, dissociative routes to alkanol activation, or different radical−surface interactions than those observed for octahedral oxides. Such effects must be taken into account to develop more universal descriptors, when such systems are used as oxidation catalysts.

4. CONCLUSIONS

C−H bond activation energies for oxidative dehydrogenation (ODH) in homologous series of alkanes (CH_4, C_2H_6, C_3H_8, *n*-C_4H_{10}, *i*-C_4H_{10}) and alkanols (CH_3OH, C_2H_5OH, 2-C_3H_7OH) with increasing degree of substitution of the C atom and in products of these reactants (C_2H_4, C_3H_6, 1-C_4H_8, CH_2O, CH_3CHO) were calculated on POM clusters ($H_4SiMo_{12}O_{40}$, $H_3PW_{12}O_{40}$, $H_4PV_1Mo_{11}O_{40}$, $H_4PV_1W_{11}O_{40}$, and $H_3PMo_{12}O_{40}$ at different O atom locations with DFT or DFT+U treatments) to examine the effect of reactant and catalyst properties on reactivity and selectivity in sequential C−H activation pathways. These calculations show that C−H activation energies decrease with decreasing C−H bond dissociation energy in reactants (smaller C−H BDE) and increasing H-abstraction strength of lattice O atoms (more negative HAE), but such effects are not monotonic due to disruptions caused by interaction energy between the organic radicals and hydroxylated surface oxygens species at the transition state. These radical−surface interaction energies become more negative for activation of C−H bonds with decreasing bond strengths in saturated alkanes and alkanols and at vinyl and carbonyl groups in alkenes and alkanals, leading to activation energies that decrease even more strongly than C−H BDE (slopes ∼1.3−1.5 for linear trends in Figure 7). In contrast, transition states for activation of C−H bonds at C atoms allylic to C═C and C═O groups in alkenes and alkanols exhibit much weaker interaction energies than nonallylic C−H bonds of similar strengths, leading to lower reactivity of such bonds than the predictions based on BDE effects alone.

Effects of reactant C−H BDE, abstractor HAE, and radical−surface interaction energies at each C−H activation transition state on activation energies are accurately described by a model based on crossing of harmonic potentials for C−H bond dissociation and O−H bond formation that accounts for a product state radical−surface interaction energy characteristic of each different type of C−H bond and the lateness of transition state. The model and data show that more exothermic reactions on stronger H-abstractors proceed via transition states that lie earlier along the reaction coordinate for C−H dissociation and O−H bond formation. These early transition states with C−H bonds cleaved and O−H bonds formed to lesser extents are less sensitive to both C−H and O−H bond strengths. As a result, these early transition states have smaller activation energy differences between reactants and primary products and thus improve selectivity to primary products when such products have weaker C−H bonds than reactants. These effects of radical-surface interactions and abstractor strengths, together with enthalpy−entropy effects at C−H activation transition states determine ratios of rate constants for activation of reactants and primary products involved in sequential ODH reactions.

■ ASSOCIATED CONTENT

Supporting Information

The Supporting Information is available free of charge on the ACS Publications website at DOI: 10.1021/acs.jpcc.6b04604.

Comparison of broken-symmetry transition state energies with their single point energies derived from triplet and closed-shell singlet calculations, effect of computational methods on C−H BDE, HAE, and activation energies, and details of enthalpy and entropy calculations (PDF)

■ AUTHOR INFORMATION

Corresponding Author

*Phone: +1-925-323-5559. Fax: +1-510-642-4778. E-mail address: iglesia@berkeley.edu.

Notes

The authors declare no competing financial interest.

■ ACKNOWLEDGMENTS

This work was supported by the U.S. Department of Energy, Office of Science, Office of Basic Energy Sciences, under Contract Number DE-AC05-76RL0-1830. Computational facilities were provided by the Environmental Molecular Science Laboratory (EMSL) at Pacific Northwest National Laboratory (PNNL), a DOE Office of Science User Facility (Proposal Number 48772) and by Extreme Science and Engineering Discovery Environment (XSEDE; Project Number TG-CTS150005).

■ REFERENCES

(1) Cavani, F.; Ballarini, N.; Cericola, A. Oxidative Dehydrogenation of Ethane and Propane: How Far from Commercial Implementation? *Catal. Today* **2007**, *127*, 113−131.
(2) Mamedov, E. A.; Corberán, V. C. Oxidative Dehydrogenation of Lower Alkanes on Vanadium Oxide Based Catalysts. The Present State of the Art and Outlooks. *Appl. Catal., A* **1995**, *127*, 1−40.
(3) Labinger, J. A.; Bercaw, J. E. Understanding and Exploiting C-H Bond Activation. *Nature* **2002**, *417*, 507−514.
(4) Tatibouët, J. M. Methanol Oxidation as a Catalytic Surface Probe. *Appl. Catal., A* **1997**, *148*, 213−252.
(5) Soares, A. P. V.; Portela, M. F.; Kiennemann, A. Methanol Selective Oxidation to Formaldehyde over Iron-Molybdate Catalysts. *Catal. Rev.: Sci. Eng.* **2005**, *47*, 125−174.
(6) Mars, P.; van Krevelen, D. W. Oxidations Carried Out by Means of Vanadium Oxide Catalysts. *Chem. Eng. Sci.* **1954**, *3*, 41−59.
(7) Chen, K.; Iglesia, E.; Bell, A. T. Isotopic Tracer Studies of Reactions Pathways for Propane Oxidative Dehydrogenation on Molybdenum Oxide Catalysts. *J. Phys. Chem. B* **2001**, *105*, 646−653.
(8) Chen, K.; Bell, A. T.; Iglesia, E. Kinetics and Mechanism of Oxidative Dehydrogenation of Propane on Vanadium, Molybdenum, and Tungsten Oxides. *J. Phys. Chem. B* **2000**, *104*, 1292−1299.
(9) Deshlahra, P.; Carr, R.; Chai, S.-H.; Iglesia, E. Mechanistic Details and Reactivity Descriptors in Oxidation and Acid Catalysis of Methanol. *ACS Catal.* **2015**, *5*, 666−682.
(10) Labinger, J. A. Oxidative Coupling Of Methane: An Inherent Limit to Selectivity? *Catal. Lett.* **1988**, *1*, 371−376.
(11) Batiot, C.; Hodnett, B. K. The Role of Reactant and Product Bond Energies in Determining Limitations to Selective Catalytic Oxidations. *Appl. Catal., A* **1996**, *137*, 179−191.

DOI: 10.1021/acs.jpcc.6b04604
J. Phys. Chem. C 2016, 120, 16741−16760

(12) Brønsted, J. N. Acid and Basic Catalysis. *Chem. Rev.* **1928**, *5*, 231−338.
(13) Evans, M. G.; Polanyi, M. Inertia and Driving Force of Chemical Reactions. *Trans. Faraday Soc.* **1938**, *34*, 11−24.
(14) Santen, R. A. V.; Neurock, M.; Shetty, S. G. Reactivity Theory of Transition-Metal Surfaces: A Brønsted-Evans-Polanyi Linear Activation Energy - Free Energy Analysis. *Chem. Rev.* **2010**, *110*, 2005−2048.
(15) Zboray, M.; Bell, A. T.; Iglesia, E. The Role of C-H Bond Strength in the Oxidative Dehydrogenation of Alkanes. *J. Phys. Chem. C* **2009**, *113*, 12380−12386.
(16) Zalc, J. M.; Green, W. H.; Iglesia, E. NOx-Mediated Homogeneous Pathways for Formaldehyde Synthesis from Methane-Oxygen Mixtures. *Ind. Eng. Chem. Res.* **2006**, *45*, 2677−2688.
(17) Gounder, R.; Iglesia, E. The Roles of Entropy and Enthalpy in Stabilizing Ion-Pairs at Transition States in Zeolite Acid Catalysis. *Acc. Chem. Res.* **2012**, *45* (2), 229−238.
(18) Döbler, J.; Pritzsche, M.; Sauer, J. Oxidation of Methanol to Formaldehyde on Supported Vanadium Oxide Catalysts Compared to Gas Phase Molecules. *J. Am. Chem. Soc.* **2005**, *127*, 10861−10868.
(19) Goodrow, A.; Bell, A. T. A Theoretical Investigation of the Selective Oxidation of Methanol to Formaldehyde on Isolated Vanadate Species Supported on Silica. *J. Phys. Chem. C* **2007**, *111*, 14753−14761.
(20) Getsoian, A. B.; Shapovalov, V.; Bell, A. T. DFT+ U Investigation of Propene Oxidation over Bismuth Molybdate: Active Sites, Reaction Intermediates, and the Role of Bismuth. *J. Phys. Chem. C* **2013**, *117*, 7123−7137.
(21) Noodleman, L.; Case, D. A.; Aizman, A. Broken Symmetry Analysis of Spin Coupling in Iron-Sulfur Clusters. *J. Am. Chem. Soc.* **1988**, *110*, 1001−1005.
(22) Carreón-Macedo, J. L.; Harvey, J. N. Do Spin State Changes Matter in Organometallic Chemistry? A Computational Study. *J. Am. Chem. Soc.* **2004**, *126*, 5789−5797.
(23) Pope, M. T.; Muller, A. Polyoxometalate Chemistry: An Old Field with New Dimensions in Several Disciplines. *Angew. Chem., Int. Ed. Engl.* **1991**, *30*, 34−48.
(24) Okuhara, T.; Mizuno, N.; Misono, M. Catalytic Chemistry of Heteropoly Compounds. *Adv. Catal.* **1996**, *41*, 113−252.
(25) Misono, M. Unique Acid Catalysis of Heteropoly Compounds (Heteropolyoxometalates) in the Solid State. *Chem. Commun.* **2001**, 1141−1152.
(26) Barteau, M. A.; Lyons, J. E.; Song, I. K. Surface Chemistry and Catalysis on Well-Defined Oxide Surfaces: Nanoscale Design Bases for Single-Site Heterogeneous Catalysts. *J. Catal.* **2003**, *216*, 236−245.
(27) Deshlahra, P.; Iglesia, E. Methanol Oxidative Dehydrogenation on Oxide Catalysts: Molecular and Dissociative Routes and Hydrogen Addition Energies as Descriptors of Reactivity. *J. Phys. Chem. C* **2014**, *118*, 26115−26129.
(28) Perdew, J. P.; Chevary, J. A.; Vosko, S. H.; Jackson, K. A.; Pederson, M. R.; Singh, D. J.; Fiolhais, C. Atoms, Molecules, Solids, and Surfaces: Applications of the Generalized Gradient Approximation for Exchange and Correlation. *Phys. Rev. B: Condens. Matter Mater. Phys.* **1992**, *46*, 6671−6687.
(29) Dudarev, S. L.; Manh, D. N.; Sutton, A. P. Effect of Mott-Hubbard Correlations on the Electronic Structure and Structural Stability of Uranium Dioxide. *Philos. Mag. B* **1997**, *75*, 613−628.
(30) Hammond, G. S. A Correlation of Reaction Rates. *J. Am. Chem. Soc.* **1955**, *77*, 334−338.
(31) Kresse, G.; Hafner, J. *Ab Initio* Molecular Dynamics for Liquid Metals. *Phys. Rev. B: Condens. Matter Mater. Phys.* **1993**, *47*, 558−561.
(32) Kresse, G.; Furthmuller, J. Efficiency of *Ab-Initio* Total Energy Calculations for Metals and Semiconductors Using a Plane-wave Basis Set. *Comput. Mater. Sci.* **1996**, *6*, 15−50.
(33) Vanderbilt, D. Soft Self-consistent Pseudopotentials in a Generalized Eigenvalue Formalism. *Phys. Rev. B: Condens. Matter Mater. Phys.* **1990**, *41*, 7892−7895.
(34) Paier, J.; Penschke, C.; Sauer, J. Oxygen Defects and Surface Chemistry of Ceria: Quantum Chemical Studies Compared to Experiment. *Chem. Rev.* **2013**, *113*, 3949−3985.
(35) Lutfalla, S.; Shapovalov, V.; Bell, A. T. Calibration of the DFT/GGA+ U Method for Determination of Reduction Energies for Transition and Rare Earth Metal Oxides of Ti, V, Mo, and Ce. *J. Chem. Theory Comput.* **2011**, *7*, 2218−2223.
(36) Jónsson, H.; Mills, G.; Jacobsen, K. W. *Classical and Quantum Dynamics in Condensed Phase Simulations*; Berne, B.J., Coccotti, G., Coker, D.F., Eds.; Kluwer Academic: New York, 1998; p 385.
(37) Henkelman, G.; Jónsson, H. A Dimer Method for Finding Saddle Points on High Dimensional Potential Surfaces Using Only First Derivatives. *J. Chem. Phys.* **1999**, *111*, 7010−7022.
(38) McQurrie, D. A. *Statistical Mechanics*; University Science Books: Sausalito, CA, 2000.
(39) Campbell, C. T.; Sellers, J. R. V. Enthalpies and Entropies of Adsorption on Well-Defined Oxide Surfaces: Experimental Measurements. *Chem. Rev.* **2013**, *113*, 4106−4135.
(40) Frisch, M. J.; Trucks, G. W.; Schlegel, H. B.; Scuseria, G. E.; Robb, M. A.; Cheeseman, J. R.; Scalmani, G.; Barone, V.; Mennucci, B.; Petersson, G. A.; Nakatsuji, H.; Caricato, M.; Li, X.; Hratchian, H. P.; Izmaylov, A. F.; Bloino, J.; Zheng, G.; Sonnenberg, J. L.; Hada, M.; Ehara, M.; Toyota, K.; Fukuda, R.; Hasegawa, J.; Ishida, M.; Nakajima, T.; Honda, Y.; Kitao, O.; Nakai, H.; Vreven, T.; Montgomery, J. A., Jr.; Peralta, J. E.; Ogliaro, F.; Bearpark, M.; Heyd, J. J.; Brothers, E.; Kudin, K. N.; Staroverov, V. N.; Kobayashi, R.; Normand, J.; Raghavachari, K.; Rendell, A.; Burant, J. C.; Iyengar, S. S.; Tomasi, J.; Cossi, M.; Rega, N.; Millam, J. M.; Klene, M.; Knox, J. E.; Cross, J. B.; Bakken, V.; Adamo, C.; Jaramillo, J.; Gomperts, R.; Stratmann, R. E.; Yazyev, O.; Austin, A. J.; Cammi, R.; Pomelli, C.; Ochterski, J. W.; Martin, R. L.; Morokuma, K.; Zakrzewski, V. G.; Voth, G. A.; Salvador, P.; Dannenberg, J. J.; Dapprich, S.; Daniels, A. D.; Farkas, O.; Foresman, J. B.; Ortiz, J. V.; Cioslowski, J.; Fox, D. J. *Gaussian 09*; Gaussian, Inc.: Wallingford, CT, 2009.
(41) Macht, J.; Carr, R. T.; Iglesia, E. Consequences of Acid Strength for Isomerization and Elimination Catalysis on Solid Acids. *J. Am. Chem. Soc.* **2009**, *131*, 6554−6565.
(42) Carr, R. T.; Neurock, M.; Iglesia, E. Catalytic Consequences of Acid Strength in the Conversion of Methanol to Dimethyl Ether. *J. Catal.* **2011**, *278*, 78−93.
(43) Deshlahra, P.; Carr, R. T.; Iglesia, E. Ionic and Covalent Stabilization of Intermediates and Transition States in Catalysis by Solid Acids. *J. Am. Chem. Soc.* **2014**, *136*, 15229−15247.
(44) Callen, H. B. *Thermodynamics and an Introduction to Thermostatistics*; Wiley: New York, 1985; pp 5−37.
(45) Henrich, V. E.; Cox, P. A. *The Surface Science of Metal Oxides*; Cambridge University Press: Cambridge, U.K., 1994; pp 14−22.
(46) Luo, Y.-R. *Comprehensive Handbook of Chemical Bond Energies*; CRC Press, Boca Raton, FL, 2007; pp 11−21.
(47) Shi, C.; Xu, M.; Rosynek, M. P.; Lunsford, J. H. Origin of Kinetic Isotope Effects during the Oxidative Coupling of Methane over a Li+/MgO Catalyst. *J. Phys. Chem.* **1993**, *97*, 216−222.
(48) Liu, J.; Mohamed, F.; Sauer, J. Selective Oxidation of Propene by Vanadium Oxide Monomers Supported on Silica. *J. Catal.* **2014**, *317*, 75−82.
(49) García-Diéguez, M.; Chin, Y.-H.; Iglesia, E. Catalytic Reactions of Dioxygen with Ethane and Methane on Platinum Clusters: Mechanistic Connections, Site Requirements, and Consequences of Chemisorbed Oxygen. *J. Catal.* **2012**, *285*, 260−272.
(50) Clarke, C. S.; Jornet-Somoza, J.; Mota, F.; Novoa, J. J.; Deumal, M. Origin of the Magnetic Bistability in Molecule-Based Magnets: A First-Principles Bottom-Up Study of the TTTA Crystal. *J. Am. Chem. Soc.* **2010**, *132*, 17817−17830.
(51) Ko, K. C.; Cho, D.; Lee, J. Y. Systematic Approach To Design Organic Magnetic Molecules: Strongly Coupled Diradicals with Ethylene Coupler. *J. Phys. Chem. A* **2012**, *116*, 6837−6844.
(52) Brook, D. J. R. Radicals, Metals and Magnetism. *Science Prog.* **1998**, *81*, 369−388.
(53) Siders, P.; Marcus, R. A. Quantum Effects for Electron-Transfer Reactions in the 'Inverted Region'. *J. Am. Chem. Soc.* **1981**, *103*, 748−752.

DOI: 10.1021/acs.jpcc.6b04604
J. Phys. Chem. C 2016, 120, 16741−16760

(54) Takanabe, K.; Iglesia, E. Rate and Selectivity Enhancements Mediated by OH Radicals in Oxidative Coupling of Methane Catalyzed by $Mn/Na_2WO_4/SiO_2$. *Angew. Chem., Int. Ed.* **2008**, *47*, 7689−7693.

DOI: 10.1021/acs.jpcc.6b04604
J. Phys. Chem. C 2016, 120, 16741−16760